IEEE Access
Multidisciplinary ⋮ Rapid Review ⋮ Open Access Journal

Received 16 October 2024, accepted 10 November 2024, date of publication 13 November 2024,
date of current version 26 November 2024.

Digital Object Identifier 10.1109/ACCESS.2024.3497654

RESEARCH ARTICLE

An Experimental Dataset for Search and Rescue Operations in Avalanche Scenarios Based on LoRa Technology

MICHELE GIROLAMI[1], FABIO MAVILIA[1], ANDREA BERTON[2], GAETANO MARROCCO[3], (Senior Member, IEEE), AND GIULIO MARIA BIANCO[3], (Member, IEEE)

[1]Institute of Information Science and Technologies "Alessandro Faedo," National Research Council of Italy, 56124 Pisa, Italy
[2]Institute of Geosciences and Earth Resources, National Research Council of Italy, 56124 Pisa, Italy
[3]Department of Civil Engineering and Computer Science Engineering, University of Rome Tor Vergata, 00133 Rome, Italy

Corresponding author: Fabio Mavilia (fabio.mavilia@isti.cnr.it)

This work was supported in part by STRIVE Project by Ministero dell'Università e della Ricerca (MUR) Ministry under Grant CUP: B53C22010110001.

ABSTRACT Wireless technologies suitable for Search and Rescue (SaR) operations are becoming crucial for the success of such missions. In avalanche scenarios, the snow depth and the snowpack profile significantly influence the wireless propagation of technologies used to locate victims, such as ARVA (in French: *appareil de recherche de victimes d'avalanche*) systems. In this work, we explore the potential of LoRa technology under challenging realistic conditions. For the first time, we collect radiopropagation data and the contextual snow profile when the transmitter is buried over a 50 × 50 m area resembling a typical human-triggered avalanche. Specifically, we detail the methodology adopted to collect data through three test types: cross, maximum distance, and drone flyover. The data are annotated with accurate ground truth which allows evaluating localization algorithms based on the RSSI (received signal strength indicator) and SNR (signal-to-noise ratio) of LoRa units. We conducted tests under various environmental conditions, ranging from dry to wet snowpacks. Our results demonstrate the high quality of the LoRa channel, even when the target is buried at a depth of 1 meter in snow with a high liquid water content. At the same time, we quantify the effects of two main degrading factors for the LoRa propagation: the amount of the snow and the liquid water content existing in the snowpack profiles.

INDEX TERMS Antenna systems, ARVA, localization, LoRa, radiowave propagation, search and rescue, unmanned aerial vehicles.

I. INTRODUCTION

Search and Rescue (SaR) operations in snowy conditions represent a challenging scenario. Ski mountaineering and winter hikers are generally equipped with a rescue kit comprising ARVA (French acronym: *appareil de recherche de victimes d'avalanche*; avalanche beacon), shovel and a probe [1]. Nevertheless, their chance to survive highly depends from the hiking companions that are required to quickly localize the ARVA signal and identify the burial location. Statistics of avalanche accidents collected over years of reporting, show that the surviving curve is limited to 15 minutes, after such threshold the probability of survival quickly decreases [2]. Two critical aspects have increased the number of reported avalanches and accidents. On the one hand, the climate change surely affects the amount and the type of snow giving rise to short time periods with very high snow precipitation. This provokes often unstable snow accumulations subject to avalanche trigger. On the other hand, the increasing number of mountaineers (skialpers, hikers etc.) further increase the probability of avalanche activation. Under this aspect, it is worth to mention that the

The associate editor coordinating the review of this manuscript and approving it for publication was Yi Ren.

majority of avalanches are triggered by humans. Therefore, it becomes crucial to train mountaineers to proper using ARVA kits and, at the same time, to investigate valuable technologies to use as companion of the ARVA localization which is based on the received strength of the magnetic field generated by the transmitting beacon [3].

We present in this work an in-depth analysis of the LoRa technology to localize victims of avalanches, as originally investigated in [4]. More specifically, we present the adopted methodology derived from a list of requirements. Data are collected in a plateau located in Col de Mez at 1870 m, Italian Dolomites. We define three test typologies: *i*) *cross*, *ii*) *max distance*, and *iii*) *UAV* (unmanned aerial vehicle) *flyover* each addressing a specific aspect. A 50 × 50 m measurement area resembling the typical area of human-triggered avalanches was selected [5]. Moreover, data are collected at different conditions. We varied not only the burial depth of the target (from 0 m, namely, Tx radio lying on the snow, to 1 m burial depth) but also the snowpack profile. In particular, we report results obtained in March 2024 during which the snow layers were mainly dry, and in April 2024 when the rise in temperatures has triggered a phase of snowpack melting. In the following, we summarize the distinguishing aspects of the proposed data collection campaign:

- We present a novel methodology for setting up a data collection campaign tailored for SAR operations in avalanche scenarios. In the paper, we detail how the testing field was set up to replicate a realistic avalanche environment. Specifically, we describe the selection of measurement points and key variables, such as antenna polarization, burial depth, and snow properties.
- The dataset includes RSSI and SNR measurements collected using LoRa technology, along with detailed snow profiles documenting the conditions during testing. These metrics were gathered from four receivers, all equipped with identical hardware and software. Additionally, the dataset includes an accurate ground truth annotation that records the precise positions of the receivers throughout the tests.
- Our analysis of the dataset highlights how varying snow conditions significantly affect signal propagation. In particular, we examine how RSSI and SNR degrade as snow conditions shift from a dry to a wet snowpack.

From our experiments we observe a significant signal attenuation caused by the increase of the burial depth and of the amount of liquid water content withing the snow layers. Nevertheless, we always measure a high quality of the LoRa signal in all the conditions, enabling to the possibility of adopting a localization algorithm based on the collected data.

II. BACKGROUND AND RELATED WORKS

In this section, we provide an overview of LoRa technology, followed by a review of related works, and finally, some details on the reference use-case.

A. BACKGROUND ON LORA TECHNOLOGY

LoRa, whose name is an acronym for Long Range, is a technology operating at the physical layer (PHY) and it is based on a modulation technique known as Chirp Spread Spectrum (CSS). The intellectual property for LoRa modulation, which was introduced in 2009, is held by Semtech since 2012. Differently from other wireless technologies, such as Bluetooth Low Energy [6], [7] and BT Direction Finding [8], LoRa is capable of covering significant distances with minimal transmission power, making it suitable for long-range communication with low energy consumption.

CSS utilizes linear frequency modulated chirp pulses, which can either be up-chirps (frequency increases over time) or down-chirps (frequency decreases over time). The data is encoded as cyclic time shifts in the baseline chirp signal. When a signal is received, it is multiplied by the baseline chirp and then processed using a Fast Fourier Transform (FFT). The FFT output shows a peak in the frequency bin corresponding to the time delay in the received chirp, thus enabling the detection of the encoded data.

A receiver that performs an N-point FFT can distinguish between N cyclic shifts, allowing it to encode $\log_2(N)$ bits per chirp. This number of bits per chirp is referred to as the Spreading Factor (SF). Consequently, a spreading factor SF* can have 2^{SF*} cyclic shifts per chirp. The key properties of CSS in LPWAN (Low-Power Wide-Area Network) applications include high sensitivity, resilience to interference, low acquisition overhead, and minimal frequency synchronization requirements.

A LoRa packet consists of a sequence of repeating chirps forming a preamble, which ends with a synchronization window and several down-chirps. An optional header follows, providing information about the bit rate and symbol rate used. The payload is CSS-encoded, and an optional 16-bit Cyclic Redundancy Check (CRC) can be appended at the end. The CSS modulation allows LoRa to achieve extended radio ranges, with typical terrestrial communication distances recorded up to 30 km in rural areas and 15 km in urban areas.

The bit rate in CSS modulation depends on three main Transmission Parameters:

- *Chirp Bandwidth* (BW). Supported bandwidths include 7.8 kHz, 10.4 kHz, 20.8 kHz, 31.25 kHz, 62.5 kHz, 125 kHz, 250 kHz, and 500 kHz.
- *Spreading Factor* (SF). LoRa supports SF values from 6 to 12, where higher SF increases sensitivity but reduces data rate.
- *Coding Rate* (CR). This represents the error correction capability and can be 4/5, 4/6, 4/7, or 4/8, with the payload typically having a CR of 4/8.

Given a bandwidth BW, the symbol rate is defined by 1/BW samples per second, and, with a spreading factor SF, each symbol has a length of 2^{SF}/BW. Since each symbol encodes SF bits, the bit rate is BW/2^{SF}·SF. Higher SF values result in lower data rates but increased sensitivity.

A relevant feature of LoRa is its duty cycle imposed by local regulation for the use of the unlicensed frequency

band. In the EU 868 MHz band, the maximum duty cycle is typically set to 1%, so that a LoRa device can only transmit for such percentage of the given timeslot. In emergencies scenarios though, such limit could potentially be avoidable [4].

Regarding the Carrier Frequency, typical LoRa hardware operates in the regional UHF bands. However, it is worth reporting that the most recent LoRa products can also operate at frequencies as high as 2.4 GHz, opening new directions for future research [9].

LoRa PHY is commonly used with the LoRaWAN MAC (Medium Access Control) layer. When the MAC is bypassed, the radio simply broadcast LoRa signals. This working mode, which is exploited in this paper, is referred to as ''LoRa-MAC'' or ''raw LoRa''.

B. RELATED WORKS

Thanks to its advantages summarized in the previous Section, LoRa SaR constitutes a significant research interest for worldwide scientists. Firstly, the characterization of LoRa fading is a crucial prerequisite for deploying effective systems, especially in the case of radiolocalization application such as SaR [10]. During recent years, several propagation models and techniques have been proposed and tested for LoRa [11], including extensive characterization of temperature and humidity effects [12]. A particular scenario of interest for SaR radiopropagation is constituted by body-UAV links [13], which can be effectively modelled through a numerical-statistical approach; this approach simulates the possible body postures and, afterwards, derives equivalent antenna gain values to account for such variability [14].

Beyond the particular LoRa radiowave propagation, the use of the protocol for radiolocation purposes poses its own relevant challenges [15]. A growing literature proposes LoRa systems that utilize several localization techniques, such as, for instance, Time Difference of Arrival (TDoA) [16], and virtual fingerprinting which, differently from classical fingerprinting, avoids to collect on-site radio map thanks to satellite data [17]. It is also possible to exploit the Transmission Parameters to enhance radiolocation; for instance, reference [18] merges SF values with RSSI data to strengthen fingerprinting. RSS-UDPG (received signal strength-based with an unknown distance power gradient) techniques are particularly promising since they do not need in-depth knowledge on the radiopropagation to be effective [19].

Despite continuous progress in radiolocation methods, accurate radiopropagation models are still generally required for deploying reliable SaR systems. Indeed, even if LoRa strengths are being further improved by researchers [20] and they are extremely valuable in most emergency scenarios, like the mountain SaR [21], the variability of LoRa propagation poses a severe constraint on the actual systems' effectiveness. Due to this variability, crucial links in proposed LoRa SaR systems could be negated such as terrestrial communication with robots [22] and/or rescue dogs [23], or even ground-air/air-ground communications with UAVs [24]. Although conservative fading estimation can mitigate this issue, the overall performance of the SaR system could result hampered.

In this context, our work addresses a relevant open issue aiming at characterizing LoRa radiowave propagation in a typical SaR scenario, when the wearer of the LoRa transmitter has to be rescued in snowy environments. Even if several LoRa datasets with data on terrestrial links and with UAV exist in the scientific literature, our work is the only dataset including through-the-snow radiowave propagation. Table 1 compares our work with the most similar datasets on the radiowave propagation existing in literature.

C. THE REFERENCE USE-CASE

The design of the data collection campaign described in this work is motivated by a critical use case for mountaineering activities, specifically SaR operations in avalanche scenario. This scenario is typical during the winter season, when specific snowpack conditions are conducive to avalanche activation.

The ARVA system can operate in two modes: send and search. In send mode, the ARVA periodically broadcasts beacon signals, while in search mode, the ARVA listens for and processes beacon messages to estimate the distance and direction to the burial location. Our use case is based on this scenario with the goal of evaluating the potential of LoRa technology to enhance the efficacy of ARVA systems. We assume that all individuals involved in a search and rescue operation are equipped with a LoRa device that can be set in both send and search modes.

We also assume that rescuers divide the search phase into different steps, as usually done during training courses. These steps range from the first signal detection, to the coarse search, and the fine-grained localization. The first signal detection phase requires listening for an initial beacon message from the buried transmitter. This phase necessitates moving along the avalanche field according to a specific pattern. The goal of the coarse search is to move as quickly as possible towards the nearby of the burial location, while the fine-grained search aims to precisely locate the victim using the probe. According to these steps, we designed a testing methodology capable of collecting data at different distances from the burial location (as detailed in Sec. III-B).

LoRa is particularly indicated for SaR applications as it is designed to transmit data at long distances with limited emission power and reduced energy consumption. Moreover, LoRa chipset are very cheap and they can be easily integrated with computational units. Lastly, the operating frequencies of LoRa in EU and US allow testing this technology without any specific permission.

III. EXPERIMENTAL DESIGN AND METHODS

We now detail the adopted methodology to design and executed the tests. We first describe the adopted hardware and then we describe the executed tests, respectively.

TABLE 1. Comparison between this work and the most similar datasets on the radiowave propagation existing in the literature.

Dataset	Year	LoRa	UAV	Through-the-Snow	Brief Data Description
This Work	2024	✓	✓	✓	LoRa signal strength in SaR with horizontal and vertical polarizations.
[25]	2023	✓	✓	✗	LoRaWAN data collection by UAV in Smart Campus, 426 sensors.
[26]	2022	✓	✓	✗	UAV-to-ground LoRa channel parameters: RSSI, SNR, packet delivery.
[27]	2021	✓	✓	✗	Two-tier NB-IoT and LoRa base stations for UAV communications.
[28]	2024	✓	✗	✗	LoRa signal strength in multi-story building for localization.
[29]	2024	✓	✗	✗	Radiofrequency fingerprinting with LoRa and Software Defined Radios.
[30]	2023	✓	✗	✗	LoRa radiowave parameters in Smart Campus with contextual sensory data.
[31]	2023	✓	✗	✗	IQ signals from Sub-GHz technologies: Sigfox, LoRa, IEEE standards.
[32]	2023	✓	✗	✗	Indoor and outdoor LoRa signal measurements with interference.
[33]	2021	✓	✗	✗	Path loss measurements with LoRa in a double-slope environment.
[34]	2023	✗	✗	✗	Indoor and outdoor terrestrial radiopropagation data, simulated and experimental.

A. HARDWARE KIT

The experimental setup uses 5 T-beam[1] Meshtastic boards (by LILYGO) which embeds ESP32 and SX1276 chipsets. Each T-beam board features a GSM/GPRS Antenna L722[2] (by LILYGO) and is powered by a 30,000 mAh power bank. Fig. 1 shows the adopted LoRa module. More specifically, the board features a System on Chip (SoC) that integrates an ESP32 processor and an SX1276 LoRa module. It also includes a GPS receiver and supports WiFi and Bluetooth connectivity. Custom Arduino-compliant firmware can be uploaded via a USB connection, utilizing the 4MB of flash memory and 8MB of PSRAM. Fig. 1c provides detailed specifications of the board used. One board acts as the transmitter while the others receive raw LoRa packets. The transmitter, placed in a waterproof bag and buried under the snowpack (see Fig. 1b), sends data to the receivers (analogous to the ARVA's send mode). Receiver boards are connected to Raspberry Pi 4 units, which log packet details (timestamp; RSSI, received signal strength indicator; SNR, signal-to-noise ratio) onto SD cards in text files. Receivers are synchronized initially via Wi-Fi and NTP protocols so that to have synchronized timestamps. Antennas are linearly polarized, and are rotated by 90° to fully analyze the electromagnetic wave propagation in the horizontally- and vertically-polarized components. Fig. 3b shows the receivers mounted on the top of a tripod for the data collection phase. We coded a custom firmware on both transmitter and receivers to send and receives LoRa messages and to log RSSI and SNR values. Based on [4], the firmware is set with the following parameters:

- Transmission Power = 14 dBm
- Carrier Frequency = 868 MHz (EU band)
- Spreading Factor = 7
- Bandwidth = 125 kHz
- Coding Rate = 4/5

We also use an Android app to record start and end times of data collection at different locations, namely the StepLogger app [35]. This app runs on a Google Pixel 6 Pro, synchronized via NTP protocol.

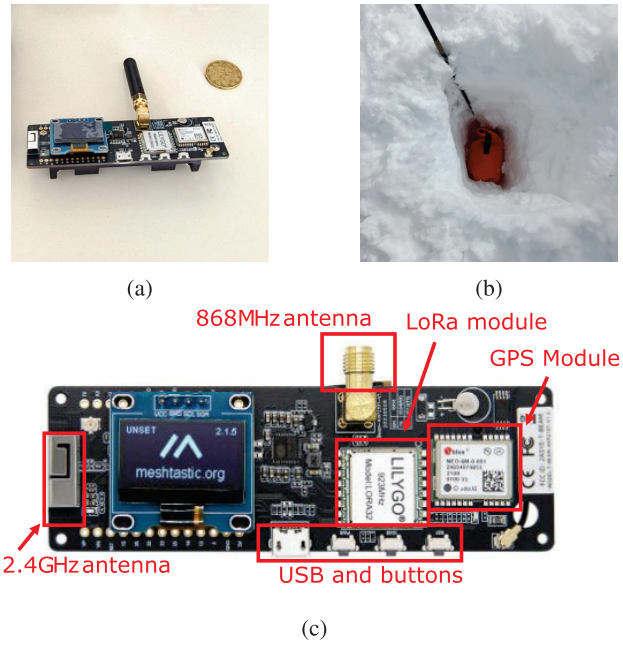

FIGURE 1. (a) The adopted LoRa module for the experimental setup; (b) the transmitter placed in a orange waterproof bag and buried under snow; (c) details of the T-Beam Meshtastic board.

Concerning tests done with the drone, we use the circular-polarized WANTENNAX005[3] antenna, produced by CaenRFID. The antenna, mounted on the bottom of the drone, as shown in Fig. 5b, allows to collect messages from transmitters in any orientation. This feature makes it particularly suitable for receiving signals from an elevated point.

B. ADOPTED METHODOLOGY AND DESIGNED TESTS

The design of the data collection has been influenced by a set of requirements, as detailed in the following.

[1] https://www.lilygo.cc/products/t-beam-v1-1-esp32-lora-module
[2] https://www.lilygo.cc/products/gsm-gprs-antenna
[3] https://www.barcodesinc.com/caen-rfid/part-wantennax005.htm?tab=product.info.accessories

- *Reproducibility*. We provide all information useful to reproduce the tests we executed and the followed methodology.
- *Multiple Receivers*. We adopt one transmitter and four receivers so that to obtain data from multiple orientations. The receivers are all identical.
- *Multiple Measurement Points*. We identify measurements points far and close from the burial location so that to reproduce coarse and fine-grained search step (as detailed next).
- *Snowpack Variability*. We collect data during different time periods in order to perform measurements with different snow types (see Sec. III-C for an extensive description of the snow profiles considered in this paper).
- *Snow Depth Variability*. We collect data with the transmitter buried at different depth so that to observe possible attenuation due to the amount of snow.
- *Aerial Data Collection*. We collect not only data for terrestrial communication, but we also investigate ground-air links by using an UAV.

Tests have been executed in a plateau located at Col de Mez, Dolomites, (Falcade, Italy)[4] at 1870 m above sea level exposed to South. The plateau is ideal for conducting the experiments as it is located in snowy area, it is easy to reach through a flat path, and snow conditions in the area greatly vary along the winter season. The plateau is also located in a safe area suitable to set up our base camp. We show in Fig. 2a the plateau where tests have been executed and, in Fig. 2b, the exact location of the identified plateau.

We design three test typologies:

- Cross test;
- Maximum Distance test;
- Drone Flyover test.

The different typologies allow observing specific aspects of LoRa signal propagation in snowy conditions as detailed in the following.

1) CROSS TEST DESCRIPTION

The **Cross** test is designed to characterize the terrestrial LoRa propagation by fixing certain *measurement points*. According to the search methodology of buried victims based on the ARVA technology, the search is organized according to different steps.

1) *Coarse search*. The surface search begins with the reception of the first signal and continues to the immediate vicinity of the buried individual. During this phase, the initial signal search method is abandoned to follow the signal path.
2) *Fine-grained search*. The surface search in the immediate vicinity of the buried person.
3) *Localization*. The initial use of the probe until it makes contact with the buried person.

[4]GPS coordinates: 46° 22'41'' N, 11°49'33'' E

According to such steps, we mark a set of measurements points of increasing distance from the burial location, each of which is a measurement point for a specific receiver. We deploy four receivers, one for each orientation: North, South, East, West. Given the burial location, we identify 40 measurements points, 10 positioned along each orientation, as reported in Fig. 3. The cross layout is composed by an outer box and an inner one.

- *Outer box*. Five measurements points, placed at: 50, 40, 30, 20 and 10 meters from the burial location along a specific orientation. Locations in this range can be used to test the coarse search step;
- *Inner box*. Five measurements points, placed at: 5, 3, 1.8, 1.2 and 0.6 meters from the burial location along a specific orientation. Locations in this range can be used to test the fine-grained and localization steps.

Given a reference location, such as 30 meters North, we collect 2 minutes of data from each receiver. Once data collection is complete, we move the receivers to the next reference location and we start a new 2-minute data collection. We also keep track of the start and end times of data collection for each reference location, as well as the actual distance to the target, this information are referred to as the Ground Truth (GT).

The transmitter is buried at different depths. During the March campaign we test three depths: 1 m, 0.5 m, and 0 m (surface; Tx lying on the snow), while during April we test 0.5 m and 0 m due to a limited snowpack. Furthermore, we vary the antenna's polarization of the transmitter and of the receivers. We measure the vertical and horizontal polarizations separately by rotating both the Tx and Rx radios by 90° in order to switch between the two polarizations.

2) MAXIMUM DISTANCE TEST DESCRIPTION

The **Maximum Distance** test is designed to measure the maximum distance at which the LoRa signal of a buried victim can be received. We acknowledge that this test can be significantly influenced by environmental factors such as trees, slopes, snow amount, and weather conditions. Nevertheless, it is useful for investigating the potential of LoRa under realistic conditions.

For the test, the transmitter is buried with horizontal polarization at the maximum available burial depth, viz., 1 m in March and 0.5 m in April. We then move away from the transmitter's location with the receiver held in hand at a height of 1.5 m above the ground. While distancing from the target, we periodically stop and collect 2 minutes data in a number of stops (or markers), as shown in Fig. 4. The maximum distance test concludes when the receiver can no longer detect any signal from the transmitter. The path followed is highly influenced by the morphology of the environment. Specifically, during our tests, we walked through a wooded area and climbed a small slope. This test serves to examine the robustness of the LoRa signal in terms of RSSI and SNR in a wide-open environment with natural obstacles.

(a) Overview of the experimental area.

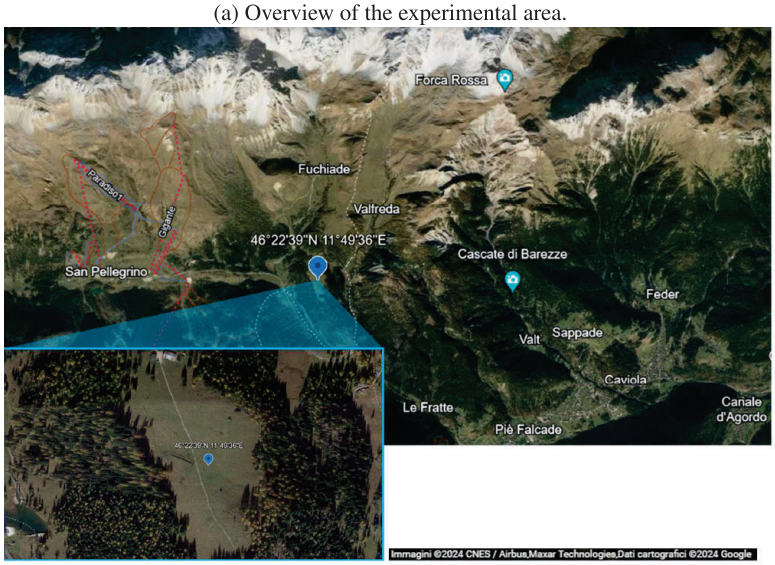

(b) Location of the experimental area.

FIGURE 2. Experimental area in Col de Mez, Falcade (BL), Italy.

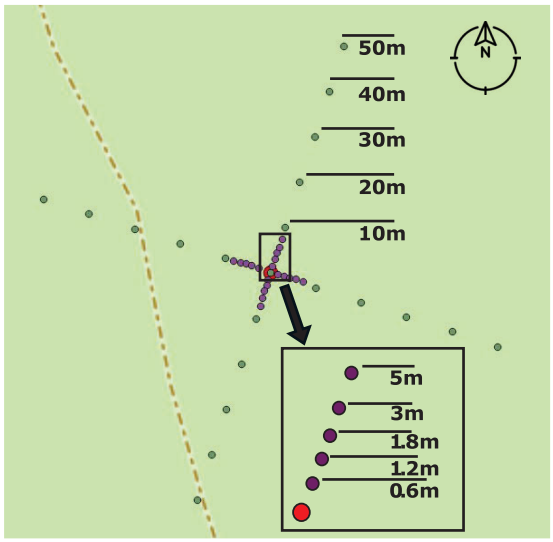

(a) Layout of the cross test.

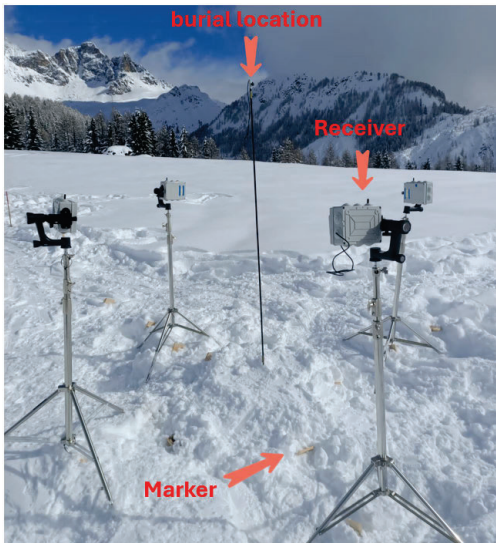

(b) Deployment of four receivers (RXs) and the transmitter (TX).

FIGURE 3. Layout of the cross test.

3) DRONE FLYOVER TEST DESCRIPTION

The **Drone Flyover** test is designed to collect data from an aerial perspective. More specifically, we organized a data collection campaign by using the quadcopter DJI Matrice 300 equipped with a LoRa receiver as payload and an omnidirectional antenna as payload (see Fig. 5b). We identify a grid of 121 measurement points covering a region of 100 m^2 centered on the burial location, with UAV flying height of 15 m. The adopted grid is shown in Fig. 5a. The first location is on the top-left corner, each row is composed

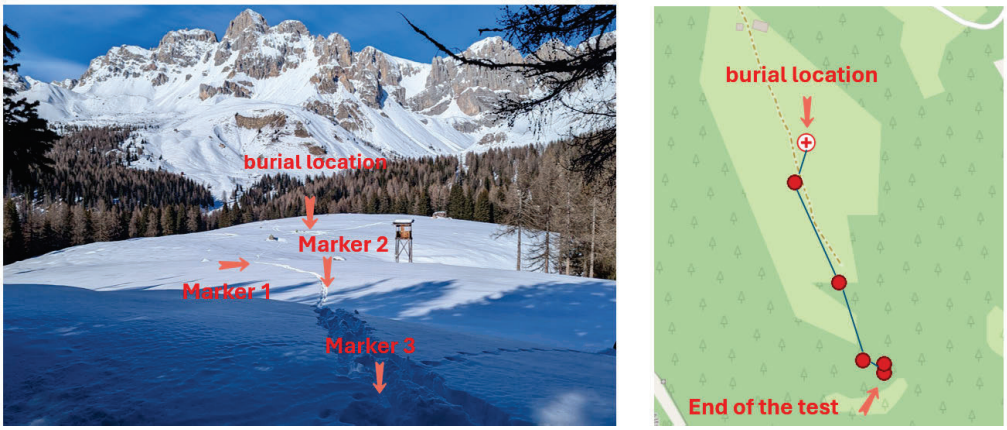

FIGURE 4. Layout of the maximum distance test.

by 11 measurements points and the path followed by the drone completed one row and then moves to the next rows according to the arrows reported in Fig. 5a. During April 2024, we run two tests. In the first test, the transmitter was buried under 0.5 m of snow, while in the second test, the transmitter was lying on the snow (0 m burial depth). In both the maximum distance and drone flyover tests, the transmitter is horizontally polarized towards the northwest in order to avoid the nulls of the dipole's radiation patterns.

The drone stops in each location of the grid for 30 seconds and then it automatically moves to the next point. The drone is always oriented toward North direction. It is important to remark that we configure the drone to automatically follow a flight plan consisting of stopping and moving from a reference location to the next one. This configuration has two benefits; on one hand the drone exploit GPS/RTK precision enabling it to hover a reference location with high accuracy, on the other hand we can focus on the GT annotation and to check the battery status of the drone and other environmental conditions. Flight plans have been designed and tested in advance before starting the data collection campaign.

Table 2 summarizes all the executed tests. Each test is labeled with an ID, the type, the date, the target's depth, the antenna's polarization and the snow condition referred to as Θ, as detailed next in Sec. III-C. Table 2 also provides details concerning the amount of the collected data for each test and the duration. In total, we collected more than 235 thousand of RSSI and SNR values, for a total duration of almost 7 hours.

C. SNOW PROFILE

In this Section, snow profiling performed by AINEVA's nivologists is described.

1) SNOW PROFILING METHODOLOGY

Nivometric profiles are performed following the International Classification for Seasonal Snow on the Ground ICSIUCCS-IACS 2009 [36] and the AINEVA Model 4 (Interregional Snow and Avalanche Association) for graphical representation. Below we provide the main observations or measurements that characterize the different layers identified within the snowpack and their meanings. Snow profiles are executed with instrumentation reported in Fig. 6.

Water content (Θ). It refers to the amount of water present in the snow in its liquid state. This parameter is synonymous with the content of free (liquid) water in a snow sample relative to its volume, which can range from 0% (dry snow) to 25% (soggy snow). The liquid water present in the snow results from melting, rain, or a combination of both phenomena. The method used for this type of assessment, which is the most widely adopted, involves an empirical measurement performed by extracting a snow sample from each identified layer, which must be compressed in the fist with a gloved hand to check for the presence of water. This operation must also be evaluated in association with the snow temperature (e.g., $T_s \leq 0\,^{\circ}$C dry snow; $T_s = 0\,^{\circ}$C wet to soggy snow) and the visual assessment of any liquid water present at the junctions between grains using a magnifying glass.

Grain shape (F). It is detailed with appropriate subclasses [36] that further differentiate the grains based on their morphology and the governing physical process. Given that each identified layer may contain two or more grain types, by convention, the predominant form is listed first, while the others are considered secondary forms. Identification is performed using a magnifying glass.

Grain size (E). The grain size of a snow layer is determined by the average size of its grains. The size of a grain or particle is measured in millimeters (mm) along its longest dimension. This measurement is performed using a magnifying glass and, when possible, with an accuracy of up to one-tenth of a millimeter.

Snow hardness (R). It represents a measure of the snow's resistance to compression by an object. Hardness values provide a relative index that varies based on both the operator and the instrument used. In this measurement campaign, snow hardness was determined using the hand test (as originally proposed by De Quervain [37]) at the layer level and horizontally along the profile. This method involves intuitively and progressively applying five different levels

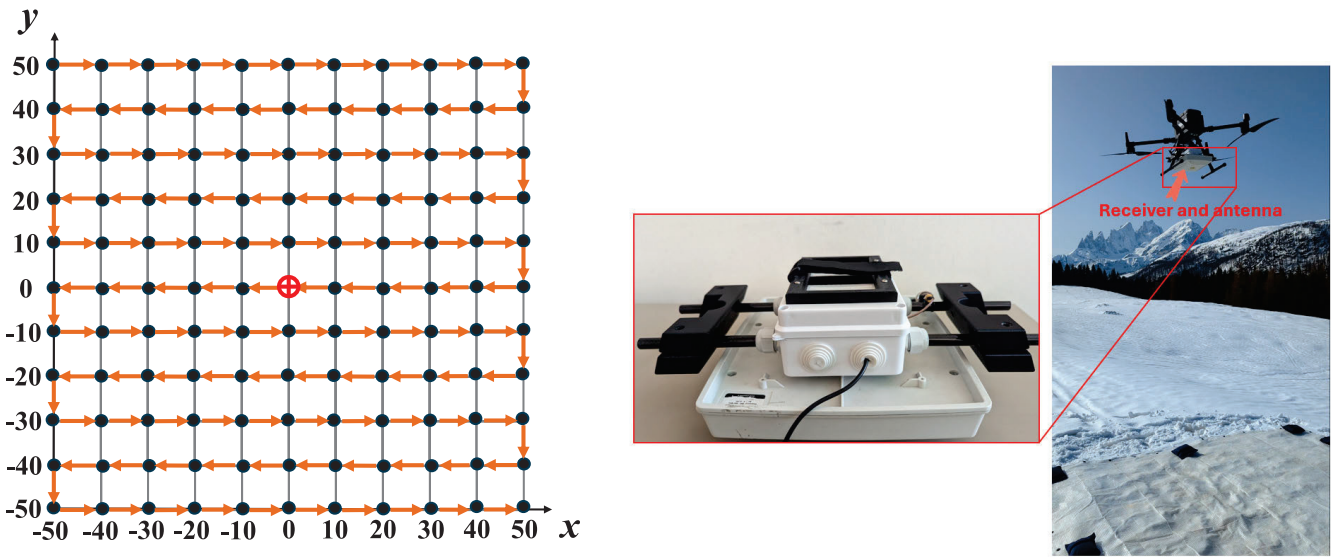

(a) Layout of the drone flyover test.

(b) Receiver deployed as drone's payload.

FIGURE 5. Layout of the drone flyover.

TABLE 2. Overview of tests executed during the data collection campaigns.

ID	Type	Date	Liquid Water Content		Target depths [m]			Polarization		Collected Values	Duration [min.]
			Dry	Wet	1	0.5	0	Vertical	Horizontal		
T1.1	Cross	March 2024	✓		✓			✓		19 249	20.08
T1.2					✓				✓	19 251	20.07
T1.3						✓		✓		19 196	20.03
T1.4						✓			✓	19 096	19.91
T1.5							✓	✓		19 242	20.07
T1.6							✓		✓	19 184	20.01
T1.7	Max distance				✓			✓		6 235	36.98
T2.1	Cross	April 2024		✓		✓		✓		20 019	20.88
T2.2						✓			✓	19 302	20.13
T2.3							✓	✓		19 628	20.46
T2.4							✓		✓	19 463	20.30
T2.5	Max distance					✓			✓	5 712	32.53
T2.6	Drone flyover					✓			✓	16 624	69.39
T2.7							✓		✓	16 403	68.44
									Total	**238 334**	**409.28**

of force, corresponding to various ranges of compression resistance: fist, four fingers, one finger, pencil, knife blade, and ice.

Snow density (ρ). It is the mass per unit volume (kg/m^3), is typically calculated by weighing a snow sample of a known volume, accounting for all snow components (ice, liquid water, and air). Density was calculated for layers with a thickness of ≥ 4 cm using a coring tube with a known volume of 1/10 liter. The sampling was done through horizontal coring in the lower third of the layer.

Snow temperature (T_S) indicates the thermal state of the snowpack at a certain height (H). By taking a series of measurements at regular intervals along the vertical axis of the snowpack, a thermal profile can be created, and a temperature gradient can be calculated. This gradient is essential for defining the thermodynamic transformations that influence the morphology and mechanical properties of the various layers. Measurements are taken along the vertical profile of the snowpack down to the snow/ground interface, with the thermometer sensor inserted horizontally at regular intervals (usually every 10 or 20 cm). Snow temperature measurements allow us to clearly distinguish between dry snow ($T \leq 0°$) and wet snow ($T = 0°$). On the graphical representation of the AINEVA Model 4, the temperature profile is depicted as a red line, with points corresponding to the heights at which measurements were taken.

Lastly, the graphical representation of the snow profile (AINEVA Model 4) provides numerous simplified pieces of information, including grain morphological classes. The various layers are depicted as a histogram, where the block height corresponds to the layer's height and its length corresponds to the measured R. Grain morphological classes

FIGURE 6. The instrumentation used for vertical analysis of the snowpack (snow profile).

can also be synthetically represented using a coded and conventional color scale. Fresh snow and recent snow in the form of precipitation particles and decomposed and fragmented particles are depicted in green. Rounded grains, typical of destructive metamorphism or wind transport, are represented in light pink. Crystals typical of constructive metamorphism are depicted in shades of blue, with faceted particles in azure and depth hoar in blue (surface hoar in magenta). Melted forms are rendered in red, with added vertical black lines for melt and refreeze crusts. The main classes are represented by color, while morphological subclasses of grains are further detailed on the side in symbolic form.

2) SNOW PROFILE ON MARCH 2024

The snow profile conducted on March 11, 2024 was performed with an overall snow height (H_S) of 116 cm, as a series of snowfall events occurred along the winter season. A significant internal warming of the snowpack is observed, with an almost isothermal snow temperature profile at around 0 °C, the highest temperature at which the snowpack can be found. The surface of the snowpack appears dry and loosely cohesive, with the first 4 cm (*H* 116-112 cm from the ground) characterized by precipitation crystals (Θ 1; *F* 1d, *E* 2, *R* 1) deposited in the previous 24 hours. The density is typical of a fresh snowfall, with ρ 100 kg/m^3. Below, there is approximately 20 cm of recent snow (*H* 112-93 cm), deposited during snowfalls from March 2 to March 6, which has started to decompose. There are two layers of dry snow, the surface layer loosely cohesive mainly composed of decomposed and fragmented particles and some rounded grains (Θ 1; *FF* 2a-3a; *E* 1-0.4; *R* 1), while between *H* 105-93 cm, there is a slightly more cohesive layer with "pellet-like" snow (Θ 1; *FF* 2a-1f; *E* 0.8-1.5; *R* 2). The densities are still relatively low, ranging from ρ 90-130 kg/m^3, typical of recent snow. Between *H* 93 cm and 82 cm, there is a layer of dry small rounded grains (*F* 3a; *E* 0.3; *R* 3), resting on a 2 cm melt and refreeze crust. Between *H* 80 cm-76 cm, there is a layer of wet snow (Θ 3), composed of melted forms (*F* 6b), with low resistance (*R* between 1 and 2). Below, there are three more resistant layers (*R* 4), with two layers composed of melted forms of wet snow (Θ 2; *H* 76-72 cm: faceted particles are also present in rounding) and an intermediate layer of dry snow of decomposed and fragmented precipitation particles (with presence of melted forms). These layers with a higher proportion of melted forms are much denser, with ρ 400-420 kg/m^3. Similarly, the layer at *H* 68-50 cm, of wet snow (Θ 2), but with a higher presence of decomposed and fragmented particles compared to the upper layers (*FF* 2a-6b; *E* 0.6-1.0; *R* 3; ρ 290 kg/m^3). In these alternating layers with a higher degree of moisture, the effect of significant warming on the snowpack, which preceded the most recent snowfalls and the drier snow visible above 82 cm, is evident. February 2024 was indeed the warmest since 1991 (with the exception of 1998), and until the 22nd the month was generally characterized by good weather. There were significant snowfall events between February 27th and 28th, with a high snow level at the end of the event (1700 m), so it cannot be entirely ruled out rain-on-snow phenomena at the site under consideration. The beginning of March was normal, with intense snowfalls on the 5th and 6th of March, with a snow level fluctuating between 600 and 1700 m.

Differently from a preliminary snow profile executed in January 2024 (not considered in this work) where faceted crystals and depth hoar were found on most of the profile, the March snowpack has undergone significant warming: the approximately 50 cm of faceted particles observed in January, characteristic of a cold and wintry snowpack, have gradually warmed and rounded, but still partly retaining their edges. We find therefore a layer of wet snow between *H* 50 and 42 cm, with melted forms and faceted particles in rounding (Θ 2; *FF* 6b-4c; *E* 2-1.5; *R* 4). Between *H* 42-25 cm, we find a heterogeneous layer, with low resistance (*R* 2), but with ice columns present (*E* 8b; *R* 4), typical of previous percolation phenomena, although the snow in this layer is, at the time of the survey, dry. The two basal layers are composed of melted forms and faceted particles in rounding (Θ 1; *FF* 6b-4c; *E* 1-2.0) with dry snow (Θ 1) and high resistance (*R* between 4 and 5). The older snow layers, which have undergone evolution compared to what was observed in the survey of January 24, 2024, have also increased in density, with a general densification of the layers, ranging from an interval of ρ 220-270 kg/m^3 in January to ρ 340-350 kg/m^3 in March (for layers characterized by kinetic growth), while the basal layer represented by a melt-freeze crust in January has changed from ρ 340 kg/m^3 to a density on March 7, 2024, of ρ 430 kg/m^3. Fig. 7 reports a detail of the snowpack stratification.

FIGURE 7. The snowpack stratification shows a clear visual distinction between the new snow deposited in the last 72 hours (surface layer *H* 116-82 cm, white color) and the old snow present before the recent snowfalls (*H* 82-0 cm, darker color).

FIGURE 8. A nivologist during snow profiling in April. In the layers near the surface (*H* 52-47 cm), there is the presence of impurities (orange color) originating from Saharan sand deposited between late March and early April 2024.

3) SNOW PROFILE ON APRIL 2024

The first half of April was extremely warm, with +6.5 ° C compared to the average calculated over the period 1991-2020, up to +10/+12 ° C above average, increasing accelerated melting of the snowpack. The melting was also favored by the abundant presence of Saharan dust, which made the surface snow red. The first days of the month were characterized by precipitation, rain even up to 2100 m altitude.

The snow profile conducted on April 11 2024, appears spring-like, with a distribution of temperatures along the vertical almost isothermal with $T_s = 0$ ° C, where all layers, due to the prolonged warming of the snowpack, have undergone the typical processes of wet snow metamorphism, with the disappearance of edges in the old snow layers and the formation of well-defined melt forms over almost the entire height of the snowpack, with snow between wet (Θ 2) and wet (Θ 3). The total height of the snowpack H_S is 57 cm, and the first 4 cm are composed of fresh, wet snow (Θ 2) and weak cohesion, fallen in the previous 24 hours. The 2 cm in contact with the air (*H* 57-55 cm) have already transformed with optimal radiation and high air temperature (T_a+9 ° C). With *H* 55-53 cm, at 11:00 hours, the precipitation particle forms are still intact, with the presence of pellet snow (Θ 2; *F* 1f; *E* 1.0; *R* 1), still warming during the profile execution. Below, almost the entire snowpack consists of melt forms, particularly rounded polycrystals, with layers of snow ranging from wet (Θ 2) to wet (Θ 3). Between *H* 53-52 cm, there is a small slightly harder layer composed of melt forms of wet snow (Θ 2; *F* 6b; *E* 2; *R* 3) which overlies a layer with a similar composition but of wet snow and lower hardness, characterized by the presence of Saharan sand, deposited with the precipitation of late March/early April (*H* 52-47: Θ 3; *F* 6b; *E* 2.0; *R* 2; ρ 490 kg/m^3). Lower down is a layer of wet snow (*H* 47-37 cm) where, in addition to melt forms, rounded grains of smaller sizes are still visible (Θ 2; *FF* 6b-3a, *E* -0.4; *R* 4; $\rho = 410$ kg/m^3).

Between *H* 37 cm and 15 cm, there are two similar layers, always composed of melt forms of wet snow, with the upper one (*H* 37-32 cm: Θ 3; *FF* 6a-6b, *E* 1.5; *R* 3; ρ 380 kg/m^3) slightly more resistant than the lower one (*H* 32-15 cm: Θ 3; *FF* 6a-6b, *E* 2.0; *R* 2; ρ 400 kg/m^3). Between *H* 15-6 cm, there are two more layers similar to the upper ones, but of wet snow (*H* 15-9 cm: Θ 2; *FF* 6a-6b, *E* 2.0; *R* 3; ρ 390 kg/m^3), with the lower layer characterized by grains still relatively small to be melt forms (*H* 9-6 cm: Θ 2; *FF* 6a-6b, *E* 0.8; *R* 2-3). At about 5 cm above the ground, there is a very hard melt and refreeze layer (*H* 6-5 cm: *FF* 6 m; *R* 5), while at ground contact there is a final layer of melt forms and wet snow (*H* 0-5 cm: Θ 3; *FF* 6a-6b, *E* 1.5; *R* 3; ρ 440 kg/m^3). As can be seen from the reported values, as the season progresses, the snow density has further increased and reached maximum values of $\rho = 410$ kg/m^3. Fig. 8 details the impurities in the snowpack due to Saharan sand.

D. DATASET FORMAT

The dataset is available to the community [38] and is organized into three folders, one for each test typology: Cross, Maximum Distance, and Drone. Each folder, except drone folder, contains the sub-folders `march` and `april`, with measurements collected in March 2024 and April 2024, respectively. The raw data consist of timeseries of values, with each row reporting values logged by a receiver, together with the GT annotations. The data format is different for

each type of test (Cross, Maximum Distance, Drone), and fields can be numeric or strings depending on the data type. First, we report in Table 3 the data structure of the Cross experimentation, where fields have the following meanings:

- `timestamp`: receiving LoRa message time in epoch format;
- `RSSI`: RSSI value in dBm;
- `SNR`: SNR value in dB;
- `receiver orientation`: one of four possible receiver orientations (north, south, east, west), as defined in Fig. 3;
- `distance`: actual distance in meters between the receiver and the burial location;
- `depth`: the burial depth in meters of the transmitter;
- `polarization`: the horizontal or vertical polarization of the receiver/transmitter.

Second, we report in Table 4 the data structure of the Maximum Distance test, where fields have the following meanings:

- `timestamp`: receiving LoRa message time in epoch format;
- `RSSI`: RSSI value in dBm;
- `SNR`: SNR value in dB;
- `depth`: the burial depth in meters of the transmitter;
- `marker ID`: the marker ID according to the path layout shown in Fig. 3;
- `longitude`: longitude of the marker ID;
- `latitude`: latitude of the marker ID.

Finally, we detail in Table 5 the data structure of the Drone test, where fields have the following meanings:

- `timestamp`: receiving LoRa message time in epoch format;
- `RSSI`: RSSI value in dBm;
- `SNR`: SNR value in dB;
- `longitude`: longitude of the drone position;
- `latitude`: latitude of the drone position;
- `x`: x-coordinate of the drone position, according to the grid shown in Fig. 5a;
- `y`: y-coordinate of the drone position, according to the grid shown in Fig. 5a;
- `depth`: the burial depth in meters of the transmitter.

Note that the Drone test was carried out only in the month of April, so the `march` subfolder is not present in the dataset.

In addition to the data collected by the LoRa receivers, we have added the complete snow profiles to the dataset, conducted in March and April, respectively. These documents are in PDF format and contain all useful nivological information, including the graphical representation of the snow profile (according to the AINEVA Model 4) and fully described in Sec. III-C.

IV. EXPERIMENTAL RESULTS

We now analyze data collected during tests described in Table 2. We study the impact of several environmental settings in order to observe significant variations of the LoRa signal propagation.

A. CROSS TEST RESULTS

First, we analyze data concerning the cross test in March and April 2024. Secondly, we compare results of the cross month-by-month.

Concerning March 2024, results of tests T1.1 to T1.6 reported in Table 2 are shown in Fig. 9a and Fig. 9b. The figures show the impact of the snow depth by varying the antenna's polarization.

Values reported in the figure are obtained by combining data from the four receivers. Concerning the RSSI (see Fig. 9a), we observe a decreasing trend as the distance from the burial location increases from 0.6 m to 50 m for all the snow depths. Specifically, tests conducted at 0 m depth yield higher median RSSI values compared to tests conducted at 1m depth. This trend is particularly evident with vertical polarization. With this polarization, at 0 m depth the average RSSI is -29.4 dBm at 0.6 m from the burial location, decreasing to -83.7 dBm at 50 m. Differently, for the same polarization but at 1 m depth, the average RSSI is -47.7 dBm at 0.6 m and -94.4 dBm at 50 m, about 12.7% more attenuation than 0 m depth.

Regarding the SNR (see Fig. 9b), no clear trend is observable since it is always reliably higher than 0 dB. However, a general observation across all tests (T1.1 to T1.6) is that the 25th percentile of SNR is 10 dB, indicating high channel quality across all distances, snow depths, and polarizations. This aspect is particularly important, as it demonstrates that the LoRa signal remains clear under variable depths, polarizations and distances from the burial location.

Regarding the effect of antenna polarization, we observe that vertical polarization tends to provide higher average RSSI values compared to the horizontal polarization across all burial depths, as shown in Fig. 10.

We further analyze the RSSI variability while varying the distance from the burial location. RSSI variability is an important features as it represents a distinguishing feature of wireless signals.

We compute the RSSI standard deviation by varying the snow depth and antenna polarization, as shown in Fig. 11.

The figure shows the median RSSI value for each location and the corresponding standard deviation depicted as a light-blue ribbon. Each row of the figure presents test results for a single polarization: horizontal and vertical, while columns display results for varying burial depths: 0 m, 0.5 m, and 1 m. Additionally, the figure includes the average RSSI value for locations in inner box (see Sec. III-B), namely those location ranging between 0.6 m and 5 m from the burial location.

Concerning the inner box, we observe an interesting trend while increasing the burial depth. Given a specific burial depth, e.g. $d = 0$ m, the average RSSI at 0.6 m from the burial location, $\mu^d_{0.6}(RSSI)$ and the average RSSI at 5 m from the burial location, $\mu^d_5(RSSI)$, its difference can

TABLE 3. Data format of values logged by receivers in Cross test.

timestamp	RSSI	SNR	receiver orientation	distance	depth	polarization

TABLE 4. Data format of values logged by the receiver in Maximum Distance test.

timestamp	RSSI	SNR	depth	marker ID	longitude	latitude

TABLE 5. Data format of values logged by the receiver in Drone experimentation.

timestamp	RSSI	SNR	longitude	latitude	x	y	depth

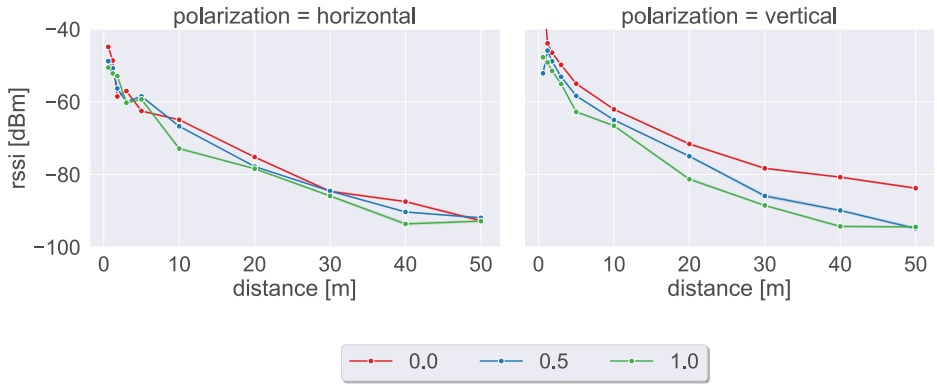

(a) Comparison of RSSI variation with respect to depths and polarization.

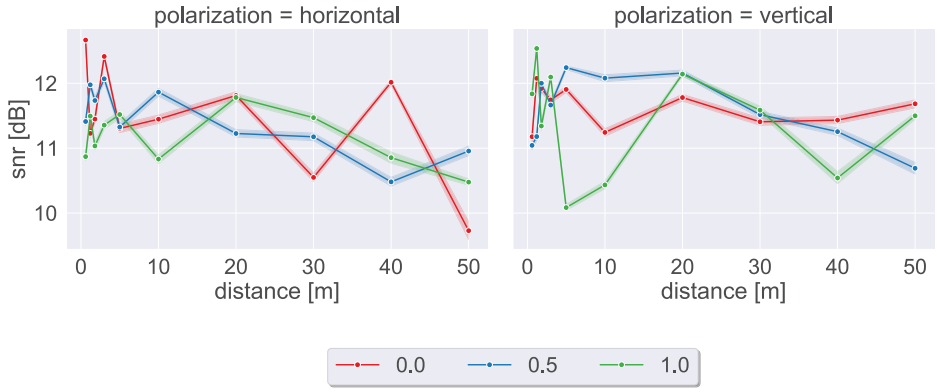

(b) Comparison of SNR variation with respect to depths and polarization.

FIGURE 9. Impact of the snow depth to RSSI and SNR for the cross test of March 2024.

be computed as $\Delta_R^d = |\mu_{0.6}^d(RSSI) - \mu_{0.6}^d(RSSI)|$. Such difference can be considered as the RSSI loss from the nearest locations from the burial depths to the limit of the inner box. We observe that such difference tends to decrease as the burial depth increases. More specifically, with horizontal polarization, $\Delta_R^0 = 17.6$ dBm while $\Delta_R^1 = 8.7$ dBm. Similarly, with vertical polarization, $\Delta_R^0 = 25.5$ dBm while $\Delta_R^1 = 15.03$ dBm. Therefore, we observe a side-effect of snow depth of reducing the RSSI variations in the inner box. Not only, but when computing the same RSSI differences for the outer box (location ranging from 10 m to 50 m), we observe that the RSSI difference in the inner box is not proportional to the RSSI difference in the outer box. Table 6 reports the RSSI loss expressed in dBm/m computed for the inner and outer boxes and for the different depths and polarizations. From the table, we can observe that the RSSI loss of the inner box is always higher with respect to the outer box and the snow depth always reduces the dBm loss per meter. Therefore the attenuation that we observe in the locations inside the inner box is higher than that the outer box. This aspect has an important consequence for the March 2024 dataset. Features of LoRa signal (RSSI and SNR) in the inner box could be more more distinguishable than that the outer box. This aspect is important as the fine-grained search in the inner box is the more critical step to find the burial location.

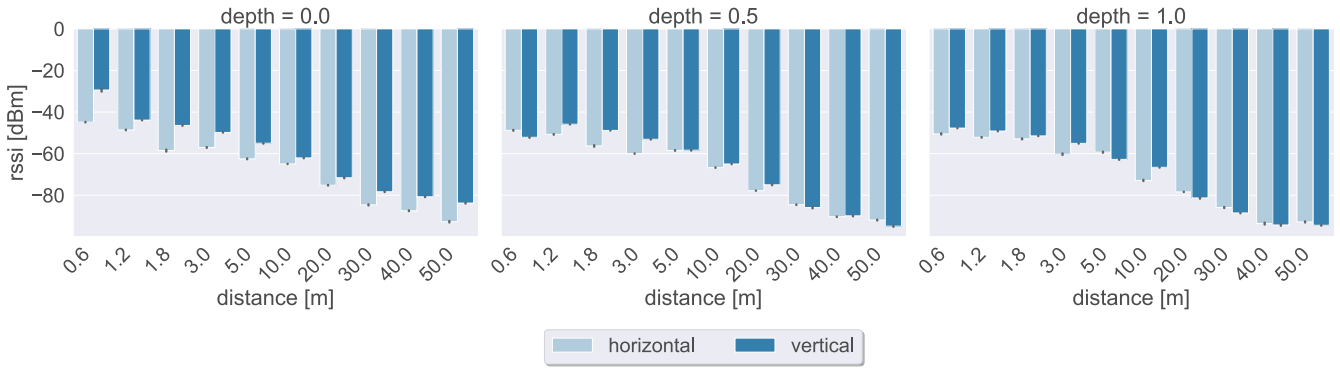

FIGURE 10. Impact of antenna's polarization to RSSI for the cross test in March 2024.

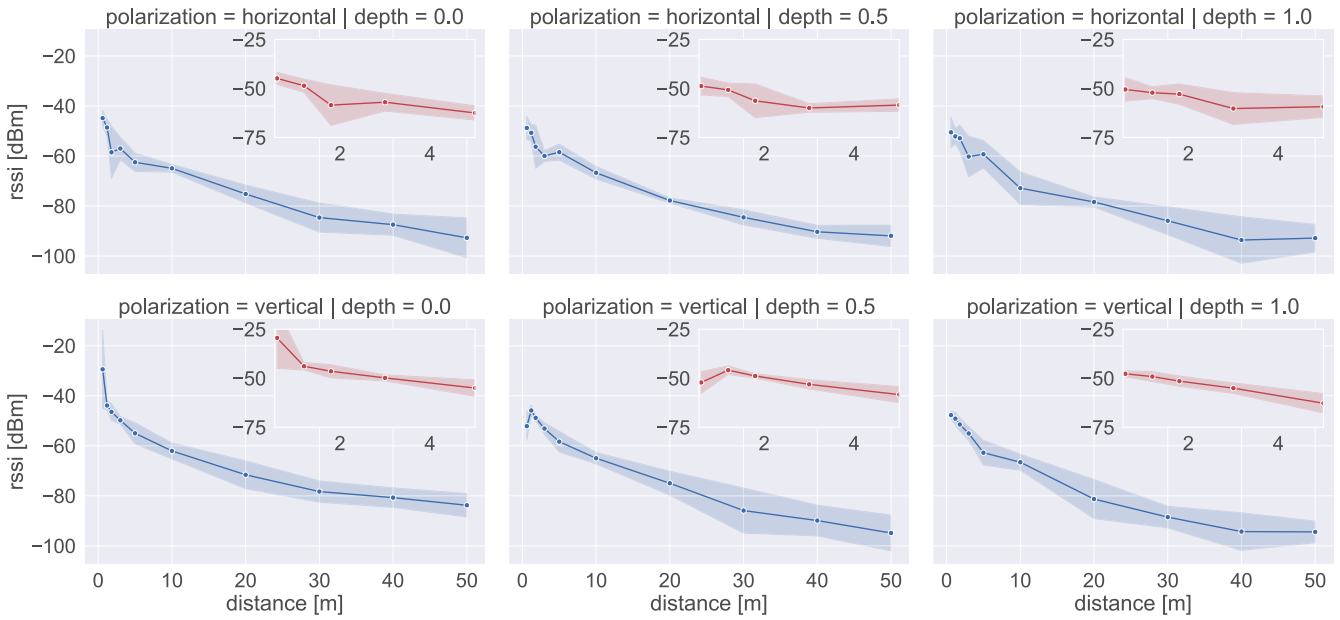

FIGURE 11. In-depth analysis of the RSSI variation for the cross test of March 2024.

TABLE 6. RSSI loss expressed in dBm/m for March and April 2024 for the inner and outer box.

Period	depth	horizontal [dBm/meter]		vertical [dBm/meter]	
		inner	outer	inner	outer
March 2024	0	4	0.69	5.8	1.3
	0.5	2.2	0.63	1.4	1
	1	1.9	0.49	3.4	1.1
April 2024	0	2.08	0.5	1.1	0.9
	0.5	4.2	0.4	2.2	1

Regarding April 2024, the results of tests T2.1 to T2.4 in Table 2 are illustrated in Fig. 12a and Fig. 12b. It is important to note that the snowpack in April 2024 is typical of the spring period, characterized by a high level of water content (Θ), as detailed in Sec. III-C3. Due to such snow conditions, only two burial depths were possible: 0 m and 0.5 m.

Similar to March 2024, the burial depth decreases the average RSSI with the cross test. This trend is observable for both polarizations, and it is even more pronounced than in the tests conducted in March 2024. More specifically, the two curves in Fig. 12 are clearly separated even with a depth difference of only 0.5 m, whereas in March 2024, the depth difference is 1 m. The SNR value does not show a clear trend, except for a steep decrease in the inner box and a slow stabilization trend in the outer box. The 25th percentile of SNR is 10 dBm, indicating high channel quality across all distances, snow depths, and polarizations.

Regarding the effect of antenna polarization, we observe that vertical polarization tends to provide higher average RSSI values compared to the horizontal polarization across all burial depths, as shown in Fig. 13. This result matches with tests executed in March 2024.

Results of the RSSI variability and its standard deviation by varying to snow depths and antenna polarization are shown in Fig. 14.

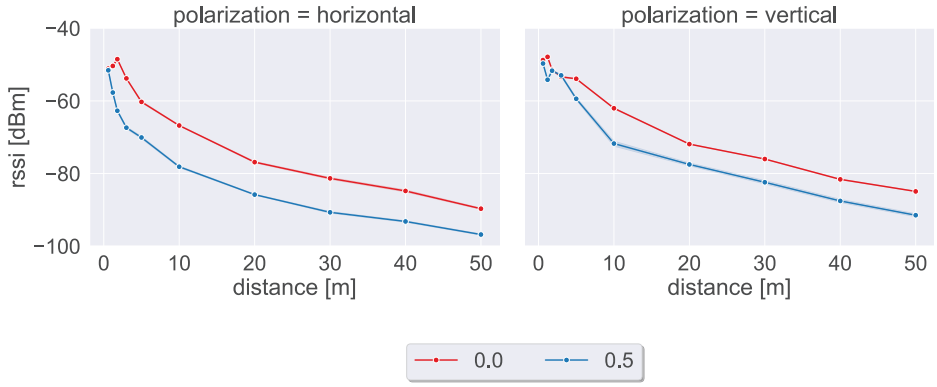

(a) Comparison of RSSI variation with respect to depths and polarization.

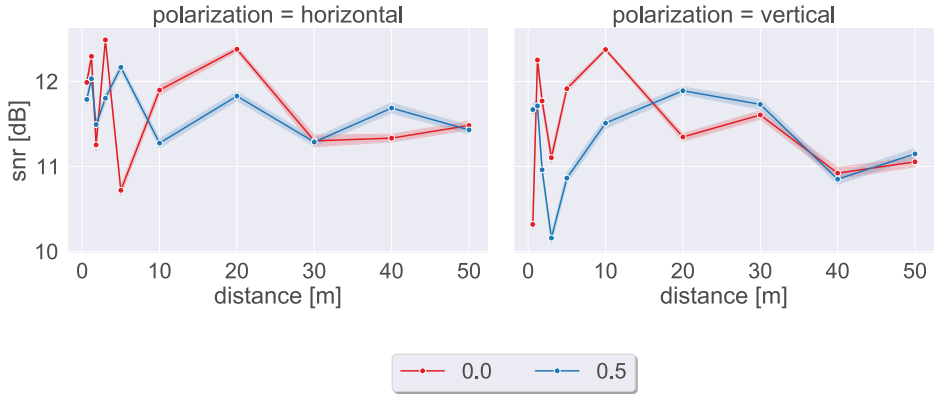

(b) Comparison of SNR variation with respect to depths and polarization.

FIGURE 12. **Impact of the snow depth to RSSI and SNR for the cross test of April 2024.**

Regarding the RSSI loss in the inner box, we observe a similar trend compared to March 2024. Specifically, with horizontal polarization, $\Delta_R^0 = 9.1$ dBm and $\Delta_R^{0.5} = 18.5$ dBm. Similarly, with vertical polarization, $\Delta_R^0 = 5.1$ dBm and $\Delta_R^{0.5} = 9.7$ dBm. Therefore, we note that snow depth has the side effect of reducing RSSI variations in the inner box. Additionally, there is no proportionality between the RSSI loss in dBm per meter between the inner and outer boxes, as reported in Table 6. An interesting case is represented by vertical polarization at 0.5 m depth. In this instance, we observe a very high variability in RSSI at every distance (0.6 m to 50 m). This trend is caused by the higher percentage of liquid water in April's snowpack compared to March 2024.

We now compare tests conducted in March and April 2024 with the goal of identifying significant differences in LoRa signal when the snowpack varies from almost dry to wet. In March 2024, tests were conducted with a snowpack that was dry in the top and lower layers ($\Theta = 1$ from 116 cm to 80 cm and from 40 cm to 0 cm) and wet in the innermost layers ($\Theta = 3 - 2$ from 80 cm to 42 cm). Conversely, in April 2024, the snowpack was wet in most of the layers ($\Theta = 3 - 2$ from 57 cm to 0 cm), resulting in higher liquid water content and potentially greater signal attenuation. Details of the snowpack profile are provided in Sec. III-C2 and Sec. III-C3.

We compare the average RSSI and SNR of the cross test by varying the month, polarization, and snow depth, as shown in Fig. 15. The graph also shows the average RSSI in the inner box (0.6 m to 5 m from the burial location), the colored ribbon show the RSSI standard deviation. From the graph, we derive two observations. Firstly, we do not observe any significant variation in the RSSI at 0 m for both vertical and horizontal polarizations. For this reason, we omit such graphs from Fig. 15. Differently, at 0.5 m burial depth some differences emerge more clearly. Specifically, the horizontal polarization at 0.5 m depth shows a clear decrease in RSSI during the April 2024 tests. Secondly, RSSI variation in the inner box differs between March and April 2024. More specifically, the April 2024 test show a reduction of average RSSI in most of the inner box's location, as shown with results of vertical polarization 0 m and 0.5 m burial depth and horizontal polarization 0.5 m burial depth. Furthermore, the RSSI loss per meter also differs between the two periods, as reported in Table 6. From the table we observe a general trend to obtain high RSSI loss per meter with tests executed in April 2024 and with 0.5 m depth. A possible justification for such variation is still the snowpack profile, that is wetter

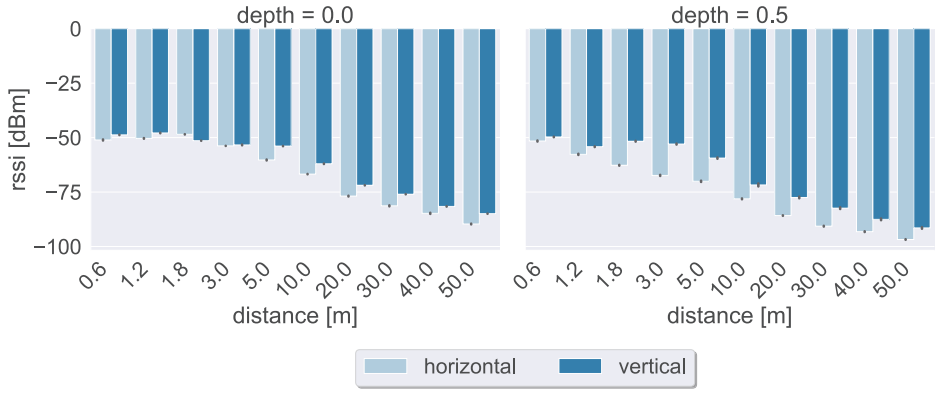

FIGURE 13. Impact of antenna's polarization to RSSI for the cross test in April 2024.

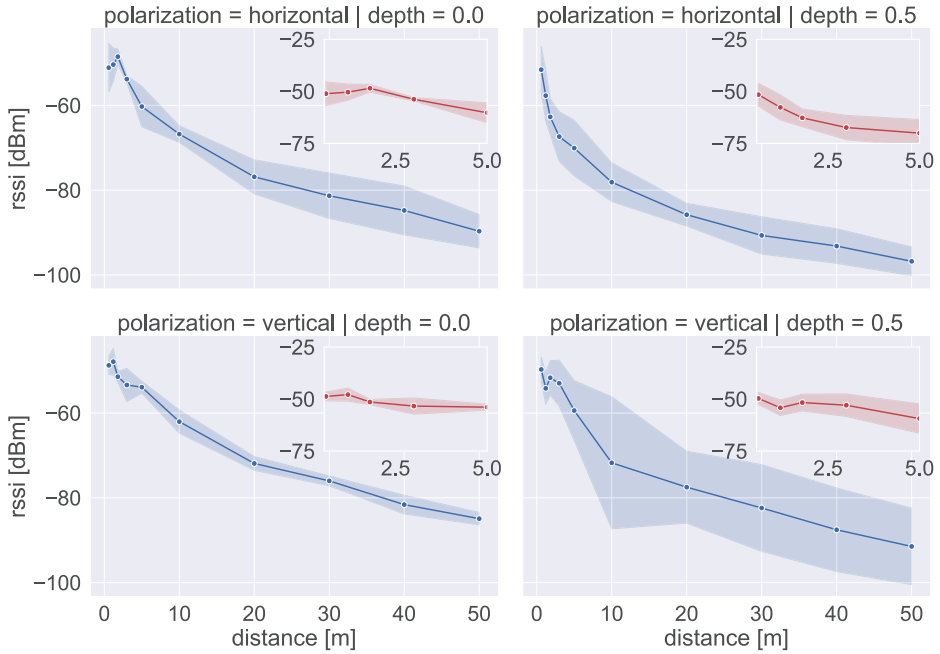

FIGURE 14. In-depth analysis of the RSSI variation for the cross test of April 2024.

in April 2024 than in March 2024. Also in this case, results obtained with the vertical polarization provide higher RSSI values than that of horizontal polarization.

Lastly, we examine the impact of the four adopted receivers. Our goal is to show a coverage map from the burial location to the maximum tested distance (50 m). Fig. 16 shows the observed map for the cross test conducted in March 2024 and April 2024 at different depths and polarizations. The figure clearly highlights regions where the RSSI is higher compared to regions where RSSI attenuates. In particular, it is possible to observe how the heatmap attenuates with tests conducted in April 2024 at 0.5 m when compared with March 2024.

The cross test reveals interesting aspects. We summarize them as follows:

- The snow depth affects the LoRa signal propagation in both March and April 2024. As expected, the deeper the burial location, the lower the signal propagation.
- The quality of the LoRa channel is consistently high in both the inner and outer boxes. This is important as it demonstrates the robustness of the channel against variations in snow depth and snowpack conditions.
- The RSSI loss per meter measured inside the inner box tends to be higher than in the outer box. This suggests that it would be valuable to further study how the LoRa signal fluctuates as it gets closer to the burial location.
- The amount of liquid water in the snowpack profile tends to attenuate the LoRa signal. Moreover, snow stratification and wave polarization have clearly observable impacts that, up to now, were only theorized. This

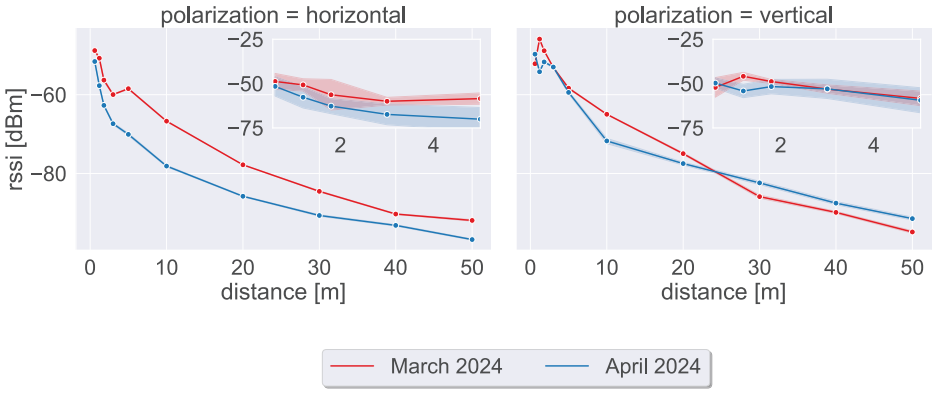

FIGURE 15. Comparison of RSSI variation of the cross test March and April 2024 at 0.5 m depth.

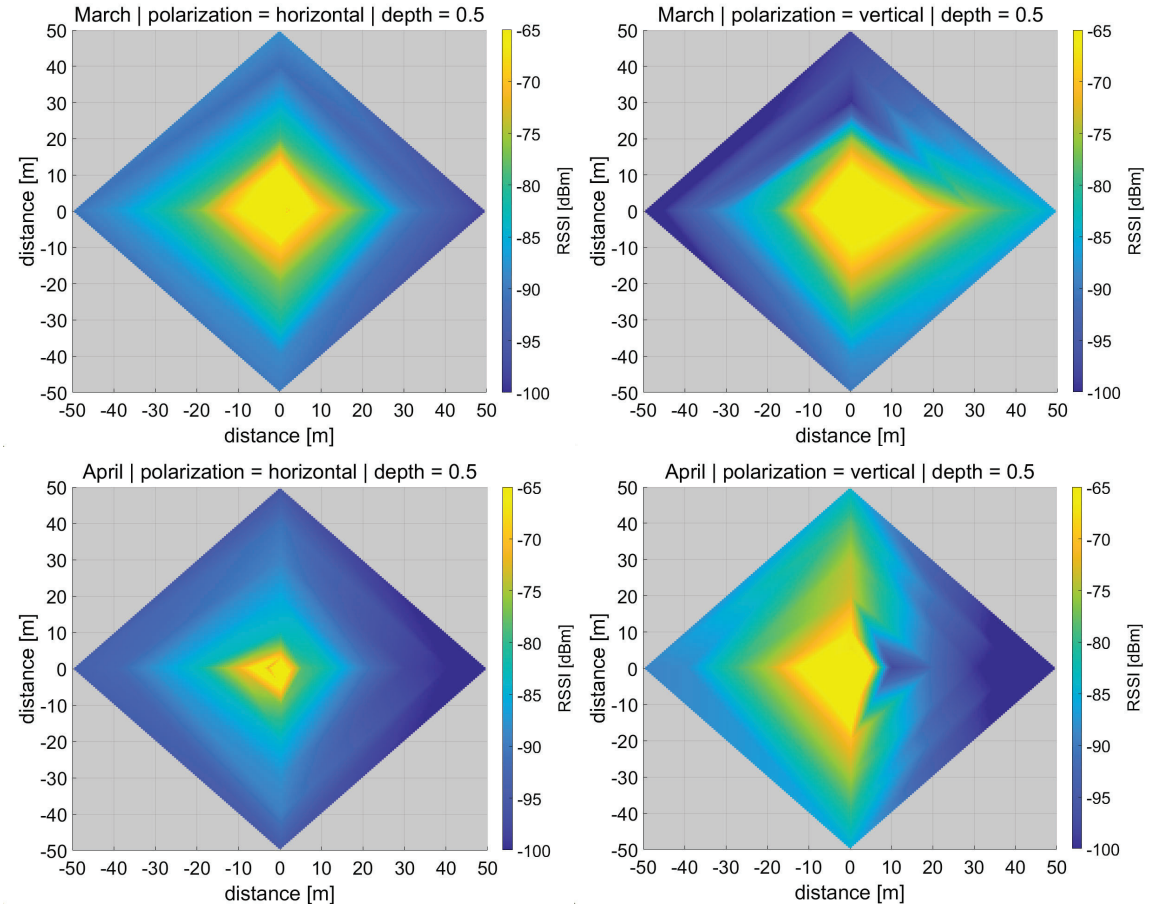

FIGURE 16. Radiation pattern of the cross test for March and April 2024.

conclusion emerges from comparing the RSSI variation in March and April 2024, but we believe more data should be collected and analyzed to further demonstrate this aspect.

- Vertical polarization provides higher RSSI values compared to tests with horizontal polarization. However, it also caused the signal to fluctuate more.

B. MAX DISTANCE TEST RESULTS

The second test we conducted has the goal of showing the potentialities of LoRa to reach long distances even in snowy conditions. As detailed in Sec. III-B, we walked along a path distancing from the burial location. We stopped in a number of markers, labeled M-1 to M-5 and we collected 2 minutes of data in each marker.

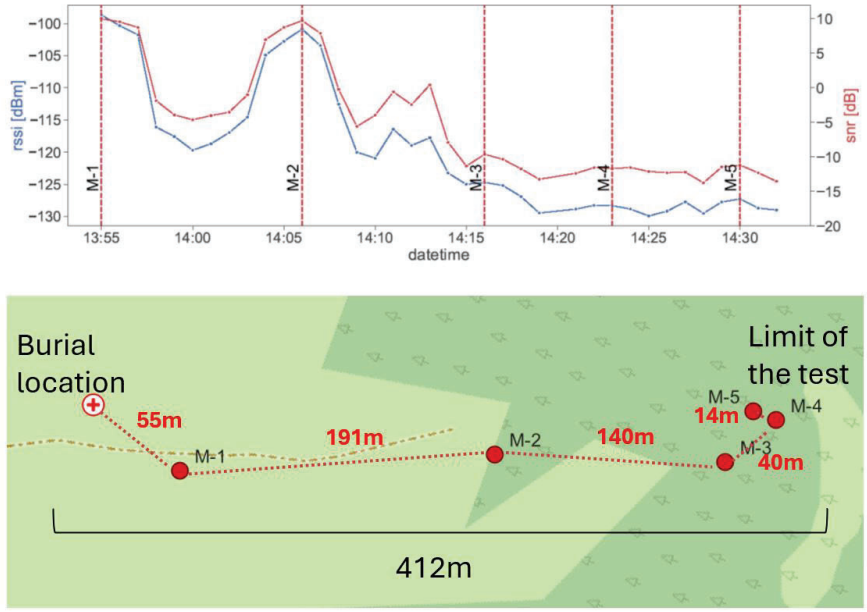

FIGURE 17. Max distance test March 2024.

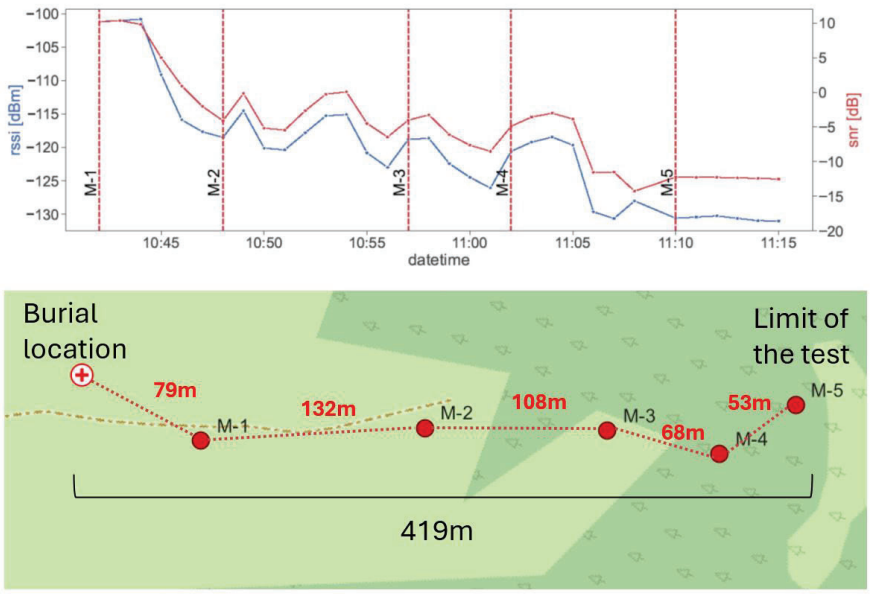

FIGURE 18. Max distance test April 2024.

Concerning March 2024 and April 2024, a graphical representation of the max distance test is shown in Fig. 17 and Fig. 18, respectively. The figures show on the top-side the RSSI and SNR variation along the followed path. The red-vertical lines show the stopping points, namely markers M-1 to M-5. The location of the markers can be found on the lowest part of the figures, where we show the path and the maximum traveled distance.

The test starts at M-1, which is about 50 m distance from the burial location. The, we walked along the plateau (see Fig. 4). During the path, we encountered a forest area and two slopes breaking the line-of-sight between the transmitter and the receiver. Data collected in each marker have been collected orienting the receiver toward the direction of the transmitter. SNR and RSSI values of LoRa signal decrease as distancing from the burial location. SNR values tend to remain stable up to a certain distance, then the SNR decreases. Concerning the March test, SNR varies between 12.7 dB in M-1 and -15.2 dB in M-5, while for the April test SNR ranges between 11.7 dB in M-1 and -15.5 dB in M-5.

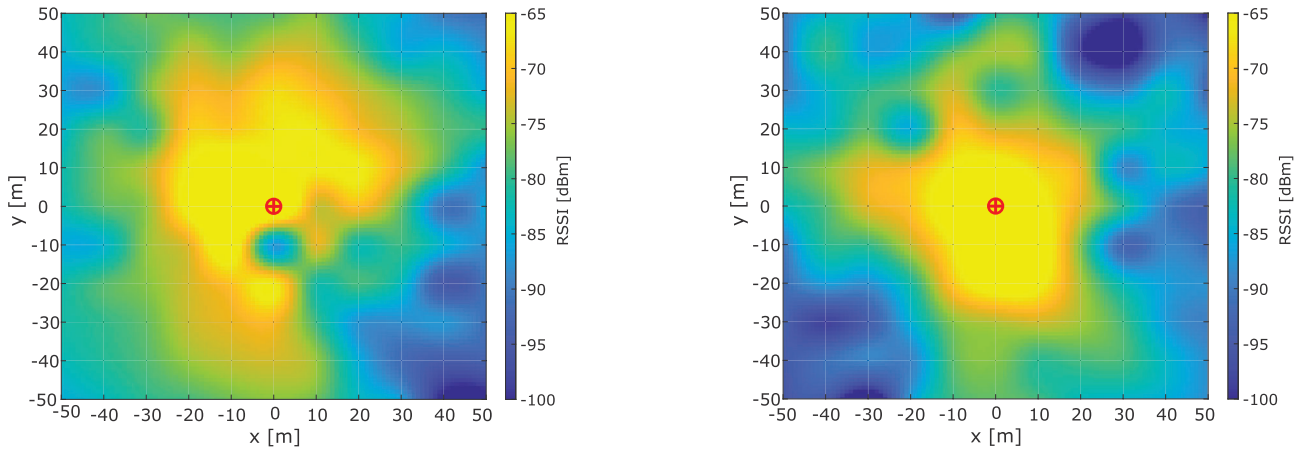

(a) Heatmap related to 0m burial depth.

(b) Heatmap related to 0.5m burial depth.

FIGURE 19. Drone Flyover test, according to the layout shown in Fig. 5. The circled red cross indicates the burial location.

In summary, we draw the following considerations from the max distance test:

- The LoRa signal can be captured at considerable distances in the considered scenario.
- The max distance test does not allow for the estimation of signal direction; rather, we only measure the RSSI and SNR. Nevertheless, the obtained results demonstrate a certain robustness against environmental obstacles such as wood, slopes, and the snowpack profile and depth.
- The results of the max distance test are highly influenced by the morphology of the testing location. In our case, the line of sight between transmitter and receiver is established only with the initial markers (e.g., M-1 to M-2).

C. DRONE FLYOVER TEST RESULTS

The last test we conducted is obtained with the adoption of a UAV, namely the DJI Matrice 300 drone, as described in Sec. III-B. Data have been collected only during April 2024, and we tested the 0 m and 0.5 m burial depths. Results are reported in Fig. 19 in which we show how RSSI varies according to the 121 sampling locations (see Fig. 5a). As expected RSSI increases while the drone flies over to the burial location, while RSSI decreases in peripheral regions. Nevertheless, the RSSI always ranges in high values from -45 dBm to -95 dBm, and we do not observe any data interruption during the tests (packet delivery ratio consistently $\sim$ 100%). The different burial depths affect the signal propagation. Indeed, the average RSSI value with 0 m depth is of -78.81 dBm, while the average RSSI value with 0.5 m depth decrease to -82.1 dBm. Furthermore, the heatmap also shows how RSSI smoothly increases along every direction (north, east, west and south).

In summary, we derive the following considerations from the flyover test:

- The adoption of a UAV to expedite the location of buried objects appears to be a promising approach. RSSI and SNR values indicate a stable and clean LoRa signal in the testing area.
- A small-size UAV can be employed to quickly delineate the burial location, for example, within a 5×5 m square region. Subsequently, such a location can be surveyed using traditional ARVA tools or a combination of LoRa and ARVA.
- The snowpack profile induces a certain degree of signal attenuation, suggesting that the liquid water content in the snow alters LoRa signal properties.

V. DISCUSSION AND FUTURE WORK

We report in this paper a data collection campaign based on the LoRa technology with the goal of evaluating its potentiality to localize a victim in an avalanche scenario. Therefore, this work represents the first step toward the performance evaluation of a localization system. Data collected in this study enable to evaluate the quality of LoRa signal under different environmental conditions. In particular, we study two orthogonal aspects affecting the LoRa signal propagation and hence the possible performance of the localization system: the snow depth and the snowpack profile. Concerning the first aspect, we varied the burial depth (from 0 m to 1 m of burial depth), while concerning the snowpack profile we tested dry and wet conditions.

The collected RSSI and SNR data show large-scale and small-scale fluctuations due to varying environmental conditions, snowpack profiles, and other factors. To perform accurate path loss and channel modeling with the provided data, these fluctuations should be averaged out by appropriate averaging widows [39], [40]. Moreover, the statistical distribution of the fluctuations should be carefully considered based on the application of interest. For instance, it can be

used to predict communication outage probability [41] and the noise affecting radiolocalization [13].

The collected LoRa data can be compared with the existing literature on radiowave propagation in a limited way, since most of the scientific analyses were performed by considering snow as a hydrometeor [42] or from remote sensing applications [43]. Standards from the International Telecommunications Union provide guidelines to account for the snow presence as hydrometeor [44] or as an obstacle on the antenna [45] and, in the most challenging system deployments, the snowy environment is accounted for by simply providing more robust communications [46], [47]. When considering only the set of reports investigating snow under or above the transmitting radio, the dataset is in line with the existing knowledge obtained through theoretical [48], simulative [49], and experimental [4], [50] analyses. Hence, the dataset described in the previous pages is suitable to be employed for channel modeling based on the several techniques described by the literature [51], [52]. Future versions of the dataset will provide more comprehensive information, allowing for more refined modeling.

The potentialities of this dataset can be enumerated as follows.

1) *Sharing a testing methodology to replicate an avalanche scenario in* safe *conditions*. More clearly, we describe in Sec. III-B the requirements and three test typologies useful to study different aspects of LoRa propagation in snowy conditions. In particular, the approach adopted to design the cross test follows the experience we gained to organize the IPIN competition (International Conference on Indoor Positioning and Indoor Navigation) [35]. This event allows researchers and industry players to test their systems at challenging conditions. We exploit such approach, to replicate in a different scenario how to collect data and how to replicate the experiments.
2) *Sharing a fully-annotated dataset*. We release the dataset with an accurate Ground Truth reporting the actual GPS coordinates of the measurement points. Such coordinates are obtained with a GPS/RTK station providing centimeter accuracy.
3) *Testing variable snow conditions*. The data have been collected at different environmental conditions, capturing significant influences caused by the amount of snow, the type of snow and the antenna's polarization. To this end, we release with the dataset standardized snow profile compiled by ARPAV Italian public entity.
4) *Localization of the burial site.* The collected data can be leveraged to implement and test localization systems aimed at determining the burial location. Specifically, RSSI-based methods using attenuation models can help identify the most probable areas where the victim may be buried. Additionally, we suggest that more advanced approaches, such as filtering algorithms (e.g., Kalman or Particle filters), can be applied to iteratively converge toward the optimal location.

We foresee some further actions able to improve the quality and the quantity of this dataset. Firstly, we plan to execute more runs of the same tests at similar conditions. This would provide more evidence of specific features that we detail in Sec. IV. Secondly, we plan to collect data during all the Winter season and not only in March and April. This action is even more challenging as snow precipitations are increasingly difficult to predict and can cause additional hardware failures. The goal is to gather additional data under snow conditions similar to those of March and April 2024, as well as new data in different snow conditions. The dataset will be accompanied by snow profiles in order to characterize the radio propagation of the LoRa signal in relation to the snow's properties.

Our intention is also to conduct new data acquisition campaigns using UAV devices. We believe the use of UAVs in search and rescue operations will become more prevalent in the future, both by rescue teams and hiking companions. Flight altitude, as well as the flight path, will be the key parameters we vary, considering the terrain's morphology and environmental conditions.

Finally, regarding weather conditions, in the next data collection campaign, we will collect environmental parameters such as temperature, humidity, and wind intensity. If possible, we also aim to vary these parameters to better characterize the LoRa signal under different environmental conditions.

ACKNOWLEDGMENT

The authors would like to thank the nivologists of ARPAV-Unità Organizzativa Neve, Valanghe e Stabilità dei Versanti-Centro Valanghe di Arabba for their valuable support during the data collection and the snow profile characterization.

The research described in this article was conducted under an agreement between the University of Rome ''Tor Vergata'' - Department of Civil Engineering and Computer Science Engineering, and the Institute of Information Science and Technologies ''Alessandro Faedo'' (ISTI) of the Italian National Research Council (CNR), researching ''Remote Radio Frequency Identification systems for Health and Safety applications through radiolocation and machine learning techniques''. Agreement duration: from September 2024 to September 2026.

(Michele Girolami and Fabio Mavilia are co-first authors.)

REFERENCES

[1] V. Ferrara, ''Technical survey about available technologies for detecting buried people under rubble or avalanches,'' *WIT Trans. Built Environ.*, vol. 150, pp. 91–101, May 2015.

[2] S. E. McIntosh, C. K. Grissom, C. R. Olivares, H. S. Kim, and B. Tremper, ''Cause of death in avalanche fatalities,'' *Wilderness Environ. Med.*, vol. 18, no. 4, pp. 293–297, Dec. 2007.

[3] N. Ayuso, J. A. Cuchi, F. Leral, and J. L. Villarroel, ''Avalanche beacon magnetic field calculations for rescue techniques improvement,'' in *Proc. IEEE Int. Geosci. Remote Sens. Symp.*, Jul. 2007, pp. 722–725.

[4] G. M. Bianco, R. Giuliano, G. Marrocco, F. Mazzenga, and A. Mejia-Aguilar, ''LoRa system for search and rescue: Path-loss models and procedures in mountain scenarios,'' *IEEE Internet Things J.*, vol. 8, no. 3, pp. 1985–1999, Feb. 2021.

[5] J. Schweizer and M. Lütschg, "Characteristics of human-triggered avalanches," *Cold Regions Sci. Technol.*, vol. 33, nos. 2–3, pp. 147–162, Dec. 2001.

[6] P. Barsocchi, A. Crivello, M. Girolami, F. Mavilia, and E. Ferro, "Are you in or out? Monitoring the human behavior through an occupancy strategy," in *Proc. IEEE Symp. Comput. Commun. (ISCC)*, Jun. 2016, pp. 159–162.

[7] F. Mavilia, F. Palumbo, P. Barsocchi, S. Chessa, and M. Girolami, "Remote detection of indoor human proximity using Bluetooth low energy beacons," in *Proc. 15th Int. Conf. Intell. Environments (IE)*, Jun. 2019, pp. 16–21.

[8] M. Girolami, F. Furfari, P. Barsocchi, and F. Mavilia, "A Bluetooth 5.1 dataset based on angle of arrival and RSS for indoor localization," *IEEE Access*, vol. 11, pp. 81763–81776, 2023.

[9] (2023). *SX1280/SX1281*. [Online]. Available: https://www.semtech.com/products/wireless-RF/lora-connect/sx1281

[10] E. AarnæS and S. Holm, "Tuning of empirical radio propagation models effect of location accuracy," *Wireless Pers. Commun.*, vol. 30, nos. 2–4, pp. 267–281, Sep. 2004.

[11] J. A. Azevedo and F. Mendonça, "A critical review of the propagation models employed in LoRa systems," *Sensors*, vol. 24, no. 12, p. 3877, Jun. 2024.

[12] T. Ameloot, P. Van Torre, and H. Rogier, "Variable link performance due to weather effects in a long-range, low-power LoRa sensor network," *Sensors*, vol. 21, no. 9, p. 3128, Apr. 2021.

[13] G. M. Bianco and G. Marrocco, "Body-UAV near-ground LoRa links through a Mediterranean forest," *IEEE Trans. Antennas Propag.*, vol. 71, no. 7, pp. 6214–6218, Jul. 2023.

[14] G. M. Bianco, A. Mejia-Aguilar, and G. Marrocco, "Numerical and experimental characterization of LoRa-based helmet-to-unmanned aerial vehicle links on flat lands: A numerical-statistical approach to link modeling," *IEEE Antennas Propag. Mag.*, vol. 65, no. 1, pp. 79–92, Feb. 2023.

[15] L. E. Marquez and M. Calle, "Understanding LoRa-based localization: Foundations and challenges," *IEEE Internet Things J.*, vol. 10, no. 13, pp. 11185–11198, Jul. 2023.

[16] T. Verbeke, E. Olti, and A. Munteanu, "Development and demonstration of a LoRa TDOA-based localisation system," in *Proc. 10th Int. Conf. Distrib. Smart Camera*, vol. 12, Sep. 2016, pp. 206–207.

[17] Y. Lin, W. Dong, Y. Gao, and T. Gu, "Sateloc: A virtual fingerprinting approach to outdoor LoRa localization using satellite images," *ACM Trans. Sensor Netw.*, vol. 17, no. 4, pp. 1–28, 2021.

[18] Y. Etiabi, M. Jouhari, A. Burg, and E. M. Amhoud, "Spreading factor assisted LoRa localization with deep reinforcement learning," in *Proc. IEEE 97th Veh. Technol. Conf. (VTC-Spring)*, Jun. 2023, pp. 1–5.

[19] G. M. Bianco, R. Giuliano, F. Mazzenga, and G. Marrocco, "Multi-slope path loss and position estimation with grid search and experimental results," *IEEE Trans. Signal Inf. Process. Over Netw.*, vol. 7, pp. 551–561, 2021.

[20] C. Bouras, A. Gkamas, and S. Aniceto Katsampiris Salgado, "Exploring the energy efficiency for search and rescue operations over LoRa," in *Proc. 11th IFIP Int. Conf. New Technol., Mobility Secur. (NTMS)*, Apr. 2021, pp. 1–5.

[21] G. M. Bianco and G. Marrocco, "Radio frequency identification and localization by wearable LoRa for search and rescue in mountains," in *Proc. IEEE Int. Conf. RFID (RFID)*, Las Vegas, NV, USA, May 2022, pp. 120–125, doi: 10.1109/RFID54732.2022.9795986.

[22] M. P. Manuel, M. Faied, and M. Krishnan, "A novel LoRa LPWAN-based communication architecture for search & rescue missions," *IEEE Access*, vol. 10, pp. 57596–57607, 2022.

[23] M. Thomeczek, "Live GNSS tracking of search and rescue dogs with LoRa," in *Proc. 43rd Real-Time Syst. Conf. Autom. Everyday Life, Real-Time*, vol. 674, 2023, pp. 115–119.

[24] Moch. Z. S. Hadi, A. A. Dafa, and P. Kristalina, "Detection of dead victims at volcanic disaster location based on drone and LoRa," in *Proc. Int. Conf. Comput. Eng., Netw., Intell. Multimedia (CENIM)*, Nov. 2022, pp. 213–217.

[25] G. Canello, S. Mignardi, K. Mikhaylov, C. Buratti, and T. Hänninen, "Data collection from LoRaWAN sensor network by UAV gateway: Design, empirical results and dataset," in *Proc. Joint Eur. Conf. Netw. Commun. 6G Summit (EuCNC/6G Summit)*, Jun. 2023, pp. 555–560.

[26] H. Aghajari, S. Ahmadinabi, H. B. Babadegani, and M. N. Soorki, "Empirical performance analysis and channel modeling of UAV-assisted LoRa networks," in *Proc. 30th Int. Conf. Electr. Eng. (ICEE)*, May 2022, pp. 463–468.

[27] S. Sobot, "VTS 2021 UAV innovation challenge—UNS," *IEEE Dataport*, 2021, doi: 10.21227/n8qa-2y02.

[28] M. A. Kamal, "Indoor localization data based on SNR and RSSI within multistory round building scenario over LoRa network," *IEEE Dataport*, 2024, doi: 10.21227/2efr-2d41.

[29] G. Shen, J. Zhang, and A. Marshall, "Radio frequency fingerprint LoRa dataset with multiple receivers," *IEEE Dataport*, 2024, doi: 10.21227/d6vx-r538.

[30] E. Eldeeb, "The smart campus dataset," *IEEE Dataport*, 2023, doi: 10.21227/xe4q-ax22.

[31] J. Fontaine and A. Shahid, "IQ signals captured from multiple sub-GHz technologies," *IEEE Dataport*, 2023, doi: 10.21227/2m0z-5s90.

[32] R. Kumar, H. P. Gupta, and R. Mishra, "Signal quality measurement (SQM) dataset," *IEEE Dataport*, 2023, doi: 10.21227/aysz-nq69.

[33] G. M. Bianco, "LoRa (868 MHz) path loss measurements in double-slope environment," *IEEE Dataport*, 2021, doi: 10.21227/agyw-ws11.

[34] K. S. Adewole, H. Olagunju, N. Faruk, A. L. Imoize, E. Alozie, O. A. Sowande, A. Abdulkarim, A. D. Usman, Y. O. Imam-Fulani, A. A. Oloyede, S. Garba, B. A. Baba, A. Musa, Y. A. Adediran, and L. S. Taura, "Terrestrial radio propagation research datasets repository," in *Proc. 2nd Int. Conf. Multidisciplinary Eng. Appl. Sci. (ICMEAS)*, Nov. 2023, pp. 1–6.

[35] F. Potortì, S. Park, A. Crivello, F. Palumbo, M. Girolami, P. Barsocchi, S. Lee, J. Torres-Sospedra, A. R. J. Ruiz, A. Perez-Navarro, and G. M. Mendoza-Silva, "The IPIN 2019 indoor localisation competition—Description and results," *IEEE Access*, vol. 8, pp. 206674–206718, 2020.

[36] C. R. L. A. Fierz, R. L. Armstrong, Y. Durand, P. Etchevers, E. Greene, D. M. McClung, K. Nishimura, P. K. Satyawali, and S. A. Sokratov, "The international classification for seasonal snow on the ground," United Nations Educ. (UNESCO), Sci. Cultural Organisation, Tech. Rep., 2009, no. 1.

[37] F. Pogue and D. McClung, "Using a thin-blade tool for measuring snow hardness and change in strength of buried surface hoar," in *Proc., Int. Snow Sci. Workshop*, 2016, pp. 589–593.

[38] M. Girolami, F. Mavilia, A. Berton, G. Marrocco, and G. M. Bianco, "An experimental dataset for search and rescue operations in avalanche scenarios based on LoRa technology," Zenodo, 2024, doi: 10.5281/zenodo.13932869.

[39] A. Grami, *Introduction To Digital Communications*. Cambridge, MA, USA: Academic Press, 2015.

[40] G. M. Bianco, A. Mejia-Aguilar, and G. Marrocco, "Low-altitude ground-UAV LoRa path loss over mountainous hills with and without snow," in *Proc. 17th Eur. Conf. Antennas Propag. (EuCAP)*, Mar. 2023, pp. 1–4.

[41] J. Seybold, *Introduction To RF Propagation*, vol. 2. Hoboken, NJ, USA: Wiley, 2005, pp. 517–526.

[42] M. M. Z. Kharadly and A. S.-V. Choi, "A simplified approach to the evaluation of EMW propagation characteristics in rain and melting snow," *IEEE Trans. Antennas Propag.*, vol. 36, no. 2, pp. 282–296, Feb. 1988.

[43] M. Tedesco and E. J. Kim, "Intercomparison of electromagnetic models for passive microwave remote sensing of snow," *IEEE Trans. Geosci. Remote Sens.*, vol. 44, no. 10, pp. 2654–2666, Oct. 2006.

[44] R. Series, *Propagation Data and Prediction Methods Required for the Design of Terrestrial Line-of-sight Systems*, document 530-18, Recommendation ITU-R, 2021.

[45] P. Series, *Propagation Data and Prediction Methods Required for the Design of Earth-space Telecommunication Systems (Question ITU-R 206/3)*, document 618-8, Recommendation ITU-R, 2023.

[46] I. Raïs, J. M. Bjørndalen, P. H. Ha, K.-A. Jensen, L. S. Michalik, H. Mjøen, Ø. Tveito, and O. Anshus, "UAVs as a leverage to provide energy and network for cyber-physical observation units on the Arctic Tundra," in *Proc. 15th Int. Conf. Distrib. Comput. Sensor Syst. (DCOSS)*, May 2019, pp. 625–632.

[47] J. Gaelens, P. Van Torre, J. Verhaevert, and H. Rogier, "LoRa mobile-to-base-station channel characterization in the Antarctic," *Sensors*, vol. 17, no. 8, p. 1903, Aug. 2017.

[48] L. Tsang and J. A. Kong, "Scattering of electromagnetic waves from a dense medium consisting of correlated mie scatterers with size distributions and applications to dry snow," *J. Electromagn. Waves Appl.*, vol. 6, nos. 1–4, pp. 265–286, Jan. 1992.

[49] V. Bataller, N. Ayuso, A. Muñoz, D. Tardioli, J. Cuchí, F. Lera, and J. Villarroel, "Modeling of through-the-snow electric field propagation for rescue systems," in *Proc. COMSOL Conf.*, Stuttgart, Germany, 2011, pp. 1–3.
[50] B. Denis, J. Keignart, and N. Daniele, "UWB measurements and propagation models for snowy environments," in *Proc. IEEE Int. Conf. Ultra-Wideband*, Sep. 2005, pp. 1–6.
[51] H. A. H. Alobaidy, M. Jit Singh, M. Behjati, R. Nordin, and N. F. Abdullah, "Wireless transmissions, propagation and channel modelling for IoT technologies: Applications and challenges," *IEEE Access*, vol. 10, pp. 24095–24131, 2022.
[52] K. Hassan, M. Masarra, M. Zwingelstein, and I. Dayoub, "Channel estimation techniques for millimeter-wave communication systems: Achievements and challenges," *IEEE Open J. Commun. Soc.*, vol. 1, pp. 1336–1363, 2020.

MICHELE GIROLAMI received the M.Sc. and Ph.D. degrees in computer science from the University of Pisa, in 2007 and 2015, respectively. He is currently a part of ISTI-CNR, as a Researcher with the Wireless Network Laboratory (WN Lab). He participates in several EU projects and national funded research projects. His research interests include indoor localization and proximity detection systems, CrowdSensing paradigm applied to edge computing and sensing technologies for pervasive computing, and the Internet of Things. He also supports the organization of the IPIN competition and he has been serving with several roles for the organization of workshops and international conferences, such as the Demo Chair for IEEE PerCom, the Program Co-Chair for IEEE ISCC, and the Workshop Co-Chair for MOCS (ISCC) and CAMAD. He served as a reviewer for numerous journals and publishers.

FABIO MAVILIA received the degree in electronic engineering from the University of Pisa, in 2012. As a member with the Wireless Network Laboratory, he currently holds the position of a Researcher with the Institute of Information Science and Technologies (ISTI), National Research Council of Italy (CNR). His research interests include the Internet of Things and cyber physical systems, with a particular focus on ambient intelligence. In particular, his work is focused on development of embedded platforms for wireless sensor networks and of algorithms for indoor activity recognition and for indoor localization, by using unobtrusive sensing devices based on radio frequency technologies.

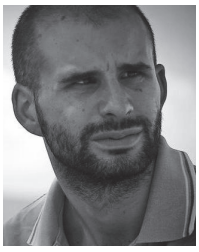

ANDREA BERTON received the degree in biomedical engineering from the University of Pisa. Since 2012, he has been specialized in the field of unmanned aerial systems (UAS), which are revolutionizing remote sensing across various scientific sectors. He is currently a Technician with the Institute of Geosciences and Earth Resources (IGG), National Research Council of Italy (CNR). His work focuses on developing acquisition methods using a range of sensors, including RGB, lidar, multispectral, thermal, and hyperspectral, applied to diverse fields, such as agriculture, cultural heritage, geomorphology, and forestry. In recent years, his efforts have increasingly targeted the study of natural resources and climate change impacts.

GAETANO MARROCCO (Senior Member, IEEE) received the M.S. degree in electronic engineering and the Ph.D. degree in applied electromagnetics from the University of L'Aquila, Italy, in 1994 and 1998, respectively. He was a Researcher with the University of Rome Tor Vergata, Rome, Italy, from 1994 to 2013, where he was an Associate Professor of electromagnetics from 2014 to 2017, has been a Full Professor since 2018, and currently the Director of the Medical Engineering School. He is the Director of the Pervasive Electromagnetics Laboratory and the Co-Founder and the President of the university spin-off RADIO6ENSE, which is active in the short-range electromagnetic sensing for the Industrial Internet of Things, smart manufacturing, automotive, and medical device. The first phase of his career was devoted to the research on time-domain electromagnetics with application to structural, broadband, and ultrawideband antennas for satellite (ESA, ASI), avionic, and naval (Leonardo) communications. Then, since 2002, he has been investigating sensor-oriented miniaturized antennas for biomedical engineering and radio frequency identification (RFID), contributing to the move from the RF labeling of objects to the passive sensor networks in the Internet of Things era. He carried out pioneering research on body-centric battery-less wireless sensors concerning textile RFID antennas, tattoo-like sensors (flexible and stretchable epidermal electronics), laser-induced-graphene wireless devices, and radio-sensors embedded inside implanted prostheses. He is listed in the PLOS ranking of the Top 2% Scientists Worldwide (source: University of Stanford). He was formerly an Associate Editor of IEEE Antennas and Wireless Propagation Letters and IEEE Journal of Radio Frequency Identification. He is also a Track Editor of IEEE Journal on Flexible Electronics and the Chair of Italian delegation URSI Commission D Electronics and Photonics.

GIULIO MARIA BIANCO (Member, IEEE) received the master's degree (Hons.) in medical engineering from the University of Rome Tor Vergata, Rome, Italy, in 2018, and the Ph.D. degree (Hons.) in "computer science, control, geoinformation" from the same University in collaboration with the Center for Sensing Solutions, European Academy (EURAC Research), Bolzano, Italy. He was a Postdoctoral Researcher with the University of Rome Tor Vergata and RADIO6ENSE srl, a spin-off of the University of Tor Vergata, from August 2021 to June 2023. Since June 2023, he has been an Assistant Professor of electromagnetic fields with the University of Rome Tor Vergata. He has authored more than 45 publications in international journals and conferences. His research interests include the modeling, development, and experimentation of wireless devices and systems. He was a member of the Youth Forum of the Pontifical Council for Culture from 2019 to 2023. His research on the modeling of wireless systems has received several awards, including the Best Ph.D. Thesis Award in Electromagnetism (2023 edition) from CNIT (Italian Inter-university Consortium for Telecommunications) and three Young Scientist Award from the International Union of Radio Science in 2020, 2022, and 2023. He served as a reviewer for numerous journals and publishers, as a TPC member and the chair for various conferences. He is also serving as an Academic Editor for the Wiley periodicals *Journal of Electrical and Computer Engineering*, *International Journal of Antennas and Propagation*, and *International Journal of RF and Microwave Computer-Aided Engineering*.

Open Access funding provided by 'Consiglio Nazionale delle Ricerche-CARI-CARE-ITALY' within the CRUI CARE Agreement